UCL Université catholique de Louvain

École polytechnique de Louvain (EPL)

Mats of LbL nanotubes for bacterial encapsulation

Dissertation presented by
Eve VERPOORTEN

for obtaining the Master's degree in
Biomedical Engineering
Option(s): Biomaterials

Supervisor(s)
Alain JONAS, Sophie DEMOUSTIER

Reader(s)
Karine GLINEL, Charles-André FUSTIN

Academic year 2017-2018

Abstract

A lack or a too low concentration of *S. epidermidis* in the biome allows colonization of the skin by pathogens and decreases the efficiency of the host for fighting back the inflammation and keeping the skin healthy. In this context, mats of membrane templated Layer-by-Layer nanotubes for bacteria encapsulation have been developed.
Nanotubes were built by the successive deposition of PAH and PSS on the wall of a porous membrane of PC. The PC was dissolved to release the tubes, and the mat was obtained by the filtration of the suspension on a PET porous membrane. The patches developed combine three nanopaper layers, first and last ones made of nanotubes only, while the layer in the middle contains in addition fluorescent latex particles, modeling the bacteria.
The first step of this master thesis was to optimize the nanotubes production process. The aim was to accelerate their build-up. Two parameters have been adjusted: the dipping time (5-10-15 min) and the number of polyelectrolytes bilayers (3-6-9). SEM observations have shown a flattening and a fusion of the tubes of three and six bilayers, while the nine bilayers tubes were well-shaped and separated. The dipping time did not have a significant influence on the morphology of the tubes. The conclusion was thus to reduce the time in solution to ten minutes while keeping nine bilayers, allowing to save 1h30 of the 6h30 initially needed for the fabrication of nanotubes.
Then, the mechanical properties of the three-layered nanopapers have been evaluated. As the mat is kept on its PET filtration membrane in a saline solution, UV-visible spectroscopy combined with fluorescence microscopy have allowed to observe that the system was decomposing, by the releasing of big chunks, while the particles were well entrapped in the network. Therefore, two methods have been suggested to consolidate the structure. The adhesion of the mat on the PET membrane was increased by coating the PET with PEI, or PEI/PSS and the cohesion of the paper was improved thanks to a $(PAH/PSS)_6$ post-coating and a PAH/PSS complexation on the three-layered nanopaper. The analyses have shown that PEI/PSS deposition enabled a better adhesion of the paper on PET than only PEI, and that the gel was the best consolidator. Tests at 37°C have revealed that the improved mat decomposes neither with the temperature.
The confirmation that the fluorescent latex particles were entrapped in the middle of the patch has been obtained by optical microscopy of thin transversal cuts of the paper, and confocal microscopy of the whole system.
Finally, a transposition to biobased polyelectrolytes has been investigated. PAH/PSS complexation has been replaced by an ALG/gCHT complexation, showing no alteration of the mechanical properties. ALG/gCHT LbL on a flat substrate has also been built to characterize the growth by ellipsometry and the roughness by AFM. An exponential growth, expected as the polymers are naturals, has been obtained.
Although further explorations, as the construction of ALG/gCHT nanotubes, and the replacement of the particles by bacteria are needed to completely develop the studied system, this work has already given keys for the design of such medical patches.

Acknowledgements

Firstly, I would like to thank my supervisors: Prof. Sophie Demoustier-Champagne, Prof. Karine Glinel and Prof. Alain Jonas. Thank you for the opportunity to work on this subject, thank you for the supervision, the support and the availability. Thank you also for the support in my procedures to get a PhD position.

I would also like to thank very much Delphine Magnin for daily support. She was a pillar for me to carry out this research. Thank you for the discussions, the formation in SEM, the planning of the work, the attentive ear and the reassuring words.

Moreover, I would like to thank all the BSMA team, for their competence, their sympathy, and their open-mindedness. Everyone is always available to help, it was a pleasure to work in this environment. Thanks to Pascale Lipnik for the microtomy, Etienne Ferain for the membranes and the porometry measurements, Elena Giol and Marie-Christine Eloy for the confocal microscopy, and also a particular thank you to Cécile D'Haese for the AFM, the help, the advices, (the nail polish for the samples,) and the discussions.

Finally, thank you to my family, and my friends, for the encouragements. Thank you to Coraline, Mathieu and Juliette for all the good time spent together working on our respective master thesis.

Contents

List of abbreviations and symbols

AAO	Anodic aluminum oxide	
AFM	Atomic force microscopy	
ALG	Alginate	
BPEI	Branched polyethylenimine	
D_0	External tube thickness	[m]
E	Young's modulus	[Pa]
gCHT	Glycol chitosan	
H	Enthalpy	[J/mol]
L	Contour length	[m]
LAP	Laponite	
LbL	Layer-by-Layer	
MMT	Montmorillonite	
M_r	Relative molecular mass	[Da]
M_w	Molecular weight	[Da]
PAA	Polyacrylic acid	
PAH	Poly(allylamine hydrochloride)	
PC	Polycarbonate	
PDADMAC	Poly(diallyldimethylammonium chloride)	
PET	Polyethylene terephtalate	
PI	Polyimide	
PLL	Polylysine	
PSS	Polystyrene sulfonate	
R_{EE}	Root-mean-square *end-to-end* distance	[m]
S	Entropy	$[\mathrm{J} \cdot \mathrm{mol}^{-1} \cdot \mathrm{K}^{-1}]$
S. aureus	Staphylococcus aureus	
S. epidermidis	Staphylococcus epidermidis	
SEM	Scanning electron microscope	
UV-spectroscopy	Ultraviolet–visible spectroscopy	
w	Wall thickness	[m]

List of Figures

List of Tables

Introduction and context

Because of their unique properties, nanostructures are at the center of attention of a lot of researches nowadays. A huge part of these researches are focused on nanofibers. They have a large length/diameter ratio, as well as a huge surface area per unit mass. They are also easily produced (template synthesis, phase separation, electrospinning, etc.) compared to other nanostructures. That makes them a good solution for applications such as tissue engineering, wound healing, sensing and catalyst. In particular, nanopapers are widely studied for these applications. [1][2]

Nanopapers can be fabricated thanks to different methods. For example, when the fibers are electrospun, the network is directly synthesized by the deposition of these fibers on the collector. Another possibility is to form the tubes, collect and suspend them and finally assemble them in a mat by filtration of the suspension liquid. LbL assembly in the nanopores of a membrane can be used to form the tubes. The membrane is then dissolved and the tubes can be collected. It allows specific properties thanks to a huge variety of material and combinations of compounds. Zhang *et al.* demonstrated two years ago the possibility to collect such tubes and then filtrate them to create nanopapers. [2]

On the other hand, skin microbiota is also widely studied for its beneficial impact on the health of the skin. It was discovered that the bacteria it contains protects the host from infections and improves the healing process. A lack of some organisms on the skin suppress their actions, and leads to diseases such as allergies, atopic eczema, psoriasis, dermatitis and acne. Therefore, new technologies that can bring back the organisms while avoiding them to enter the body are searched. [3][4]

Objectives and strategy

In this context, this work aims at developing 3-layered nanopapers containing bacteria in the middle layer. The technology developed allows to bring back the good aspects of the bacteria on the skin. Indeed, the porosity of the nanotubes mat enables the diffusion of the active agents produced by the bacteria. The 3-layered nanopaper also prevents the bacterial proliferation and dispersion, thanks to the nanotube network. In this work, bacteria were replaced by latex particles to simplify the manipulations.

The method demonstrated by Zhang *et al.* was used for this work: nanotubes were assembled on the pores of a membrane, they were then collected by dissolving the membrane, transfered in water and finally filtrated to form a mat. Three mats were filtrated on top of each other, making a three-layered nanopaper. In the nanotube suspension in water of the middle layer, before filtration, latex particles were added to model the bacteria. The

resulting structure is shown in figure 1.

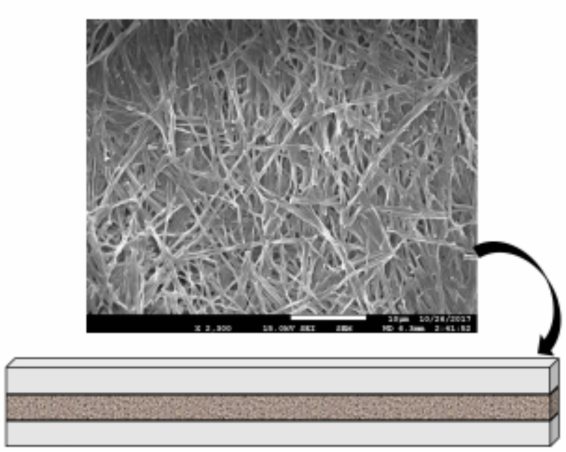

Figure 1: Structure of the paper: 3 films of PSS/PAH nanotubes on the top of each other. The one in the middle contains particles. Typical SEM image of mat.

Report structure

This report is divided into three parts. The first chapter collects the information obtained in the literature about skin microbiota, LbL assembly on flat surfaces, nanotubes construction thanks to LbL, and their collecting in nanopapers. The second chapter of this report concerns the materials and methods used. The synthesis of the nanotubes, their transfer in water and the fabrication of single or three-layered nanopaper are explained, as well as the techniques used to characterize the samples. Finally, the third chapter presents the results obtained all along this research, as well as the discussions of these results. The chapter is divided into three parts: the first part is about the parameters of the nanotubes and the single-layered mat built-up. Then, mechanical properties and temperature stability of the three-layered nanopaper are shown, as well as their improvement. The localization of the particles in the paper is determined. The last part of the chapter is about a transposition to biobased polymers. Finally, the work is ended by a summary of the main conclusions of the research and some future perspectives for the design of the application are presented.

Chapter 1

State of the art

1.1 Skin microbiota and its benefits

Just after birth, humans start sharing a complex relationship with micro-organisms present on their skin and their mucous membranes. This mixture, which is evolving throughout one's life and which is different for each person, is composed in majority by bacteria, microbes and fungi, residents or transitory. Although it has already been studied extensively, skin microbiota composition is not well-known yet. However, the researches widely focused on the bacterial part, initially to understand the potentially pathogenical behaviour of the organisms and now more and more because of the beneficial functions it can have.

Microbiota is commonly thought to be a synonym of pathogens, or of opportunist or symbiotic organisms. For example, *S. epidermidis* is well known for the infections it can produce in case of entering the body (catheters, implants). To protect itself from antibiotics and immune system, the bacteria can form biofilms, helping it to set into the body. However, skin microbiota also plays an important role in the skin's health. Its sole existence protects the host from infections. The skin represents a hostile medium because of the variations of temperature and pH, the lack of nutrients (only perspiration, sebum and skin constituent elements can supply them), the high concentration in salt and the random exposition to the sun. By consuming the resources on the skin and providing inhibition factors, micro-organisms of the microbiota prevent the invaders' colony growth. The healing process is also improved by the presence of bacteria on the skin, due to the stimulation of antibody, interferon and cytokine production as well as phagocytosis. The presence of the microbiome on the skin is therefore essential, given the fact that it protects it from infections and colonization by a pathogenic bacteria.[3][4][5]

Our microbiota evolves throughout our life, but also evolves with our environment. With the societal changes, new diseases and allergies were discovered. They probably are provoked by the alteration of the microbiota composition. These societal changes mainly correspond to the increase of the life expectancy, discovery and use of antibiotics and modification of the environment. Moreover, the human's hygiene has a huge impact on the biodiversity of the community of our skin. By bathing ourselves more, and worse, with antibacterial soaps we could suppress species of microorganisms on our skin. However, the loss of the microbiota could cause skin diseases, such as atopic eczema, psoriasis, dermatitis and acne. It is therefore important to understand and to know the benefits of the skin microbiota to be aware of the danger we are facing if we remove it from the skin.[3][4]

1.2 Encapsulation methods

These last years, encapsulation of living organisms methods were widely studied for applications such as pharmaceutical ones or food technologies. Encapsulation provides a beneficial micro-environment, which protects the organism from contamination, temperature, dryness, UV-light and mechanical stresses. It is also possible to encapsulate the organism with nutrients, forming "mini-fermenters", aiming at maintaining the metabolic activity. Depending on the material used for the encapsulation, the cells may be released: the material can be biodegradable or can offer the possibility for cells to grow out of the matrix. Diverse techniques of encapsulation were developed, this section will describe the main methods. [6]

1.2.1 Dripping

Dripping method consists of extruding a liquid through a nozzle, and then harden the droplet to form a suitable structure. For hardening, different techniques can be used. The simplest one is based on the properties of gelation of polymers such as agarose or gelatin under a huge decrease of temperature. A warm solution of polymer containing the organisms to be encapsulated is dropped into a cold collecting solution. Under the change of temperature, the material gel and therefore form a capsule. [6] [7]

Ionic gelation can also be used to harden the drops (figure 1.1). Full beads are made by dropping a polyuronic acid solution containing the organism in a solution of divalent cation. These cations diffuse through the drop and react with the negatively charged chains, forming a rigid structure. The cross-linking occurs from outside to inside. If the solutions are interchanged (divalent cation solution containing the cells dropped into polyuronic acid solution), hollow beads are formed. In this case, the cross-linking occurs from inside to outside. [6] [8] [9] [10]

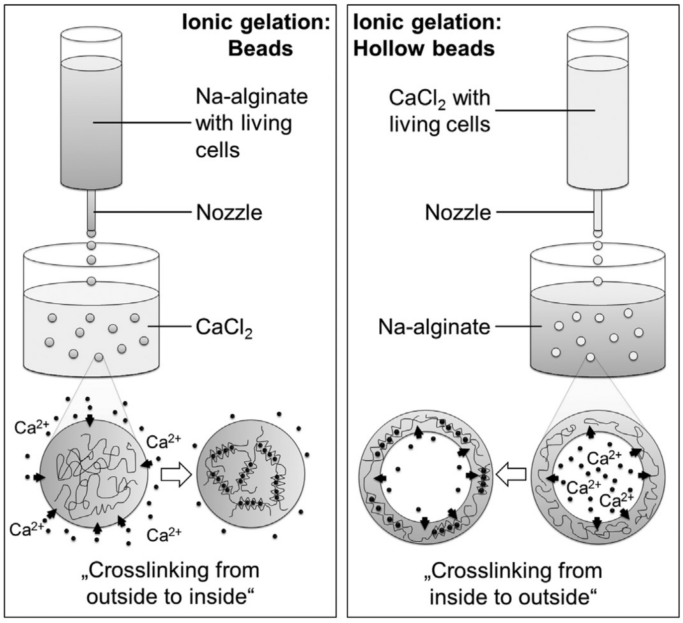

Figure 1.1: Encapsulation methods based on dripping: production of beads (left) and hollow beads (right) obtained by ionic gelation. [6]

The formation of a complex between two oppositely charged polyelectrolytes is another method to harden the drops. A positively (negatively) charged polyelectrolyte containing the organism is dropped into a negatively (positively) charged one. An ionic reaction between the two polyelectrolytes occurs at the surface of the droplet, and a semipermeable membrane is therefore formed. [11]

The advantages of dripping are the simplicity and the low particle size distribution. However, the method is limited by the speed of droplet formation and large beads are obtained. [6]

1.2.2 Emulsification

Emulsification method provides a larger size distribution, but smaller particles compared to dripping methods. It can also be easily adapted at a larger scale. A core material is emulsificated in a non-miscible phase, and the droplets are collected after solidification. The organism is miscible in the material, and therefore is entrapped in the droplets. For solidification, thermal gelation, ionic gelation or interfacial polymerization are used. For ionic gelation, a salt is present in the solution with the cells and the core material. After emulsification, an acid is added in the non-miscible phase to change the pH of the droplets, releasing the ions that will cross-link the polymer. For interfacial polymerization, a hydrophilic monomer is emulsificated and then, another hydrophilic monomer is added with a catalyser to perform the reaction. [6] [12] [13]

1.2.3 Coating

Polyelectrolytes with opposite charges are used to coat the organism forming an encapsulation shell. Either a complex is formed above the beads by dipping them in two oppositely charged polyeletrolytes bath, or a Layer-by-Layer film is formed by successive deposition of polyanion and polycation layers on top of each other. The coating offers the advantage of a complete encapsulation of the body, since each cell in suspension is coated sequentially. [14] [15]

1.2.4 Electrospinning

Cells can also be encapsulated in electrospun fiber network. The ultrafine polymer-based fibers form a porous structure with a large surface-to-volume ratio, beneficial for applications such as bioremediation. Figure 1.2 shows the process used by Gensheimer *et al* to encapsulate cells in the fibers. The cells were added to the electrospinning solution after encapsulation in hydrogel microparticles (emulsification and thermal gelation). Then the solution was electrospun towards a collector, forming the fiber network [16]. It is also possible to encapsulate directly the cells in the fibers (without hydrogel capsule), as Tong *et al.* did (figure 1.3) [17]. [18] [19]

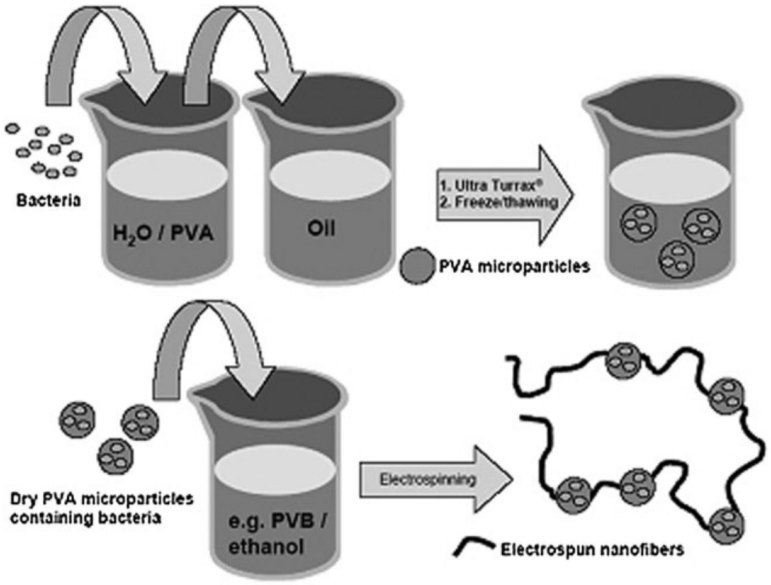

Figure 1.2: Scheme for the preparation of polymer nanofibers containing hydrogel microparticles with living bacteria by electrospinning. [16]

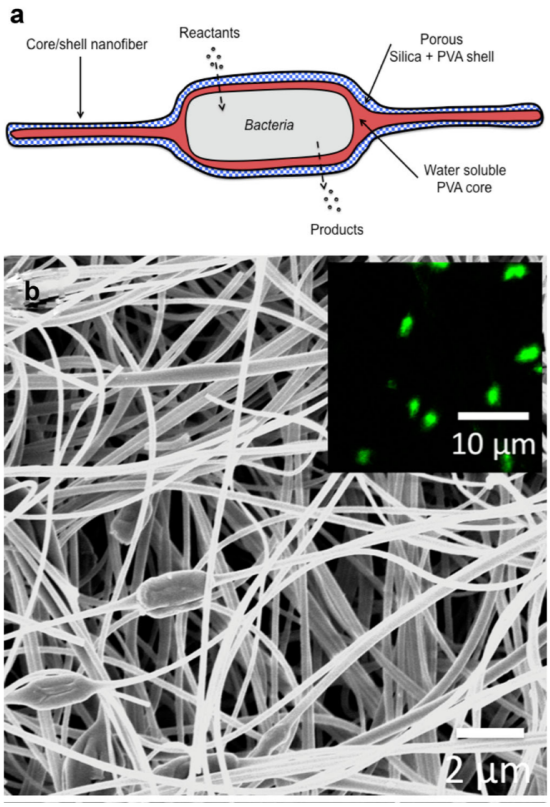

Figure 1.3: **a:** Nanofiber architecture comprised of a bacterium encapsulated in a water soluble PVA core and a silica-based porous shell surrounding the core. **b:** SEM micrograph and confocal microscopic image of the electrospun fibers that contain encapsulated E. coli expressing. [17]

1.3 Layer-by-Layer assembly technique

1.3.1 Overview

20 years ago, Moehwald, Decher, and Lvov introduced the Layer-by-Layer (LbL) bottom-up technique. Since then, LbL has been at the center of attention of a lot of studies aiming at developing nano-scale applications. It was first used as a coating method, but because of its simplicity, robustness, versatility, low-cost and easily reproducibility, it can be used in many other fields. Biomedical applications represent an important one. Indeed, LbL is used for drug delivery, cell attachment control, biosensors, biomedical technologies development, etc. [20]

The technique is based on the successive adsorption of interacting species' layers on a substrate that can bind them. These species are called building blocks. After each deposition, loosely attached molecules are cleared away by rinsing the on-growing film. By starting over n times the cycle, one can construct a n-bilayer film. Every bilayer consists of one layer of the first building block and one layer of the second one. So doing, thin pellicle are produced, but 3D geometries can also be achieved using templates, as described in section 1.3.6. In order to improve the stability of the layers, they can be cross-linked, but as it was not used in this work, details are not described here.

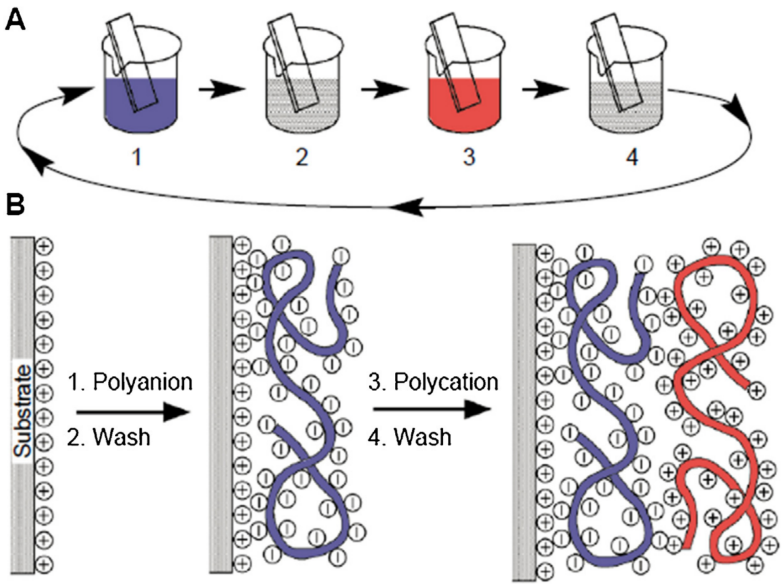

Figure 1.4: N-bilayer LbL deposition process: dipping of the substrate in solution of interacting species (steps 1 and 3), with intermediate dipping into rinse solution (steps 2 and 4). [21]

Figure 1.4 represents most common type of LbL processing, but spin-coating or spraying methods can also be applied in order to build films. Spin-coating consists of dropping the material on a rotating frame, that distributes the liquid on the whole surface and let the liquid evaporate; while a vaporizer is used in spraying LbL method to depose the building blocks on the surface. The two methods require also a washing step. The technologies associated with spin-coating and spaying are more complicated, more difficult to scale-up and more expensive, but they are material and time sparing in comparison to the

dipping method. [22]

A board range of materials can be used as substrate and also as building blocks, as long as they interact with each other. However electrostatic attraction from polyelectrolytes is the most common driving force, hydrogen bonding, charge transfer, hydrophobic, covalent and host-guest interactions can also be used. In particular, hydrogen bonding is also widely used, because it is reversibly sensitive to the surrounding environment, allowing film modification by changing the conditions. Nonetheless, films formed using hydrogen bonds as driving force are also less stable than the ones formed from electrostatic interactions. pH modifications can also control the stability of a polyelectrolyte multilayer. Indeed, the amount of net charge carried by the polyelectrolytes is affected by the pH and their ability to stick together is thus influenced. This pH effect can be used in order to control drug release from capsules, for example. Other parameters have an influence on the morphology of the film, as explained in section 1.3.4. [20]

In this work, materials used were synthetic polyelectrolytes Poly(allylamine hydrochloride) (PAH) and Poly(styrenesulfonate) (PSS) as well as biobased polysaccharides alginate (ALG) and glycol chitosan (gCHT). Therefore, the following text will focus on the Layer-by-Layer dipping technique with electrostatic interactions as driving force.

1.3.2 Polyelectrolytes as building blocks

Polyelectrolytes represent the category of polymers, synthetic or natural, that can ionize when immersed in water or solvent, by dissociating in charged polymeric chains and counter-ions. The surface on which the LbL grow is dipped into a polyanion or polycation solution, one after the other. They adsorb on the top of the substrate, because of the electrostatic interactions between them, and the counter-ions are released in the solution (figure 1.5). The deposition provokes a surface charge reversal at each step. This charge reversal is only possible if there is an overcompensation: an excess of charge in the solution compared to the amount of oppositely charged component present on the previous layer. This excess of charge allows the adsorption of a sufficiently large amount of ions. [23]

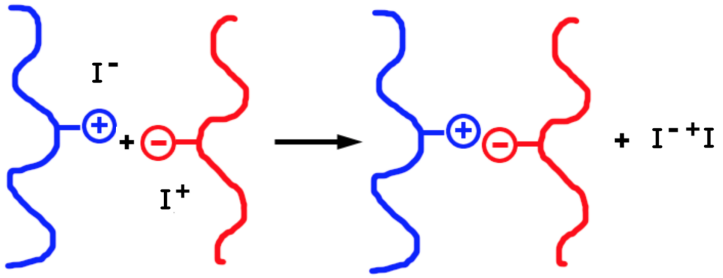

Figure 1.5: Complexation between positive polyelectrolyte and negative polyelectrolyte segments, and release of the counter-ions in the solution. Adapted from reference [24].

Thermodynamics and ion-exchange model

It is useful to have an idea of how the adsorption of polyelectrolytes will affect the enthalpy (H) and the entropy (S) in order to understand the polyelectrolytes Layer-by-Layer growth and modulation. In the first state, the counter-ions and the polyelectrolytes are free to move in the solution, while in the second state, the polyelectrolytes are adsorbed

on the oppositely charged surface.

Lets first consider H, the enthalpy. H increases thanks to the free energy liberated by the compensation of the charges. However, it cannot be the only reason why polyelectrolytes layers are assembled. Indeed, the same effect on ΔH can be achieved by the bringing together of counter-ions and polyelectrolytes in the solution. This assembly, however, does not lead to an adsorption on the substrate or last polyelectrolyte layer. It can be considered that the counter-ions compete with the opposite charges of the surface. Moreover, only enthalpic contribution cannot clarify the reversal of the surface charge, which requires a too high energy. Indeed, following this theory, there is no reason explaining why there would be more molecules hanging on the surface when its net charge would have reached zero. In conclusion, enthalpy alone cannot explain the adsorption of the polyelectrolytes process and therefore, the entropy has to be taken into account.

The first contribution to the entropy is due to the decrease of mobility of the chains, and their flattening. It corresponds to a loss of entropy during the adsorption, which can, again, not provoke the construction of the film. However, when polyelectrolytes adsorb on the surface, they release their counter-ions. (Remember that the ions compete with the polyelectrolyte of the surface.) The gain of entropy from the liberation of the counter-ions overcompensates the loss due to the adsorption of the polyelectrolytes and this contribution finally can explain the adhesion of one more layer on top of the substrate or on the preceding oppositely charged layer. [23][25]

This entropy-based explanation is called *Ion-exchange model*. It is quite simple, and describe well the effect of ionic strength or of polyelectrolyte charge density on the Layer-by-Layer technique. But due to its simplicity, it is not infallible. For example, it cannot explain why the process is irreversible. Other models more complex exist but they will not be described here. [26]

1.3.3 Kinetics and mechanism of growth

As already mentioned in section 1.3.2, overcompensation is necessary in order to reverse the surface charge, and to continue the polyelectrolyte multilayer growth. It determines the amount of adsorbed material on the next layer, and influences the size of the successive layers. Indeed, it was shown that the thickness of the film depending on the amount of bilayer can be linear, exponential or even include a transition between the two types of development. By looking at the kinetics and the mechanism of growth of the polyelectrolytes LbL film fabrication method, these phenomena can be explained. [27]

In the first minutes of the surface dipping in a polyanion or polycation solution, a rapid mass deposition occurs. The diffusion of the polymeric chains through the solution controls the rate at which this deposition occurs. The second step corresponds to the rearrangement of the chains into the deposited layer. Since complete reorganization can last for hours or even days, it is never performed entirely before the dipping into the following polyion solution. As a consequence, the chains anchor at the surface with only a few points, and the parts in between are loops and tails shaped (figure 1.6). These loops and tails bring the excess of charge leading to the charge reversal of the surface. [26]

Note that there is also a chain interpenetration during the LbL process. Indeed, as a polyion does not create a new flat and well-designed interface when it is deposited, the

next polyion will interdigitate with the preceding one. [28]

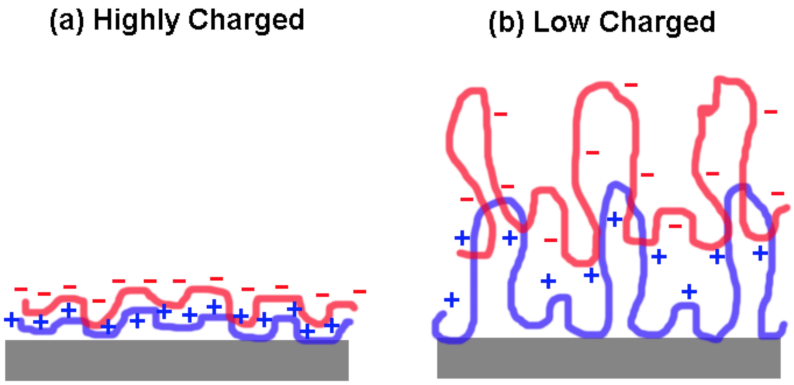

Figure 1.6: Illustration of the effect of electrical charge density of polyelectrolyte chains on the buildup of the polyelectrolyte multilayers. Highlighting of the loops and tails. [24]

The template surface and polyelectrolyte strength is determinant for the thickness of the deposition. Indeed, with strongly charged top layer, loops and tails are narrower because of the strong electrostatic interactions. The overcompensation is also smaller, leading to less material adsorbed on the next layer. If the surface is lightly charged, the chains are looser, and the layer is thicker. Fewer attractions also imply higher diffusion of the chains *in-and-from* the layers. [27]

All of these considerations influence the growth law. Strong polyelectrolytes, typically synthetic ones, follow a linear growth, since it is dominated by electrostatic interactions. Exponential growth regime corresponds to weaker polyelectrolytes, natural ones, like polysaccharides, proteins or polypeptides. Lavalle *et al.* proposed a model to explain the exponential behavior, based on the aforementioned *in-and-from* layer diffusion of the polyions. They consider that some chains are free to diffuse into the already constructed polyelectrolyte multilayers. When the film is dipped in a solution of polycations, for example, free chains of polyanion from the multilayers will diffuse toward the surface and form complexes with the polycations of the solution. Then, when all the charges are compensated, polycation free chains will finally diffuse through the film, creating the overcompensation. When the substrate will be in contact with the next solution (polyanion), the polycations will diffuse out, form new complexes, and polyanions will enter in. The thicker the film when the layers are deposited, the larger the amount of free chains and of complexes, leading to the characteristic exponential growth of the film. [29]

It is important to keep in mind the two different regimes of growth, since two kinds of polycation/polyanion couple were used in this work. First, weak PAH with strong PSS, both synthetic polyelectrolytes, following a linear growth as already reported in the literature, and then, weaker and rarer ALG/gCHT combination, expecting to grow exponentially since they are biobased polymers.

1.3.4 Parameters influencing the building of the film

Polyelectrolyte multilayer thickness, stability and permeability can be tuned by modifying the processing conditions. Among them, the salt type and concentration in the polyion solutions, the pH, the temperature, the molecular weight and the deposition time. This

section aims at giving an idea on how these parameters alter the film.

Ionic strength

Ionic strength produces the opposite effect of the strength of the polyelectrolytes (figure 1.7).

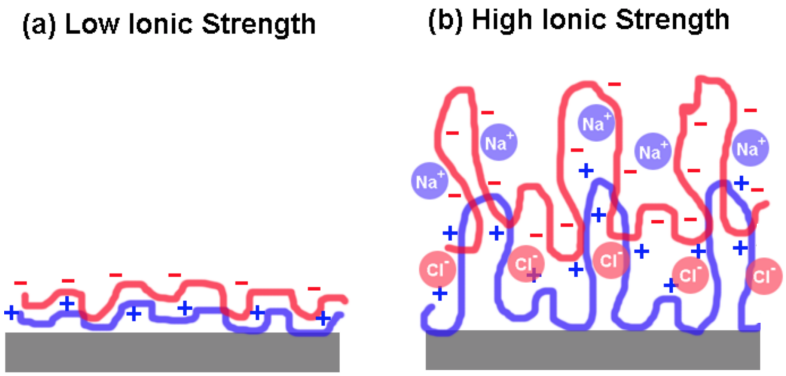

Figure 1.7: Illustration of the ionic strength effect on the conformation of adsorbed polyelectrolyte chains during the LbL assembly. [24]

Depending of the counter-ion concentration, the chains can adopt a globular coil or an extended rod configuration in the solution, because of the ability of the ions to screen the charges. At high salt concentration (high ionic strength), polymer are coiled shaped, while at low concentration they are uncoiled. The thickness of the layer corresponds to the radius of gyration of the coil. More coiled the shape, thicker the layer. Another way to say the same thing is to state that the interactions (polymer-surface and polyanion-polycation) are decreased when the ionic strength increase and thus more loops and tails can form, leading to a thicker layer. Note that a too high salt concentration can lead to a desorption of the chains. [20][24][30]

Xiangyang Shi *et al.* revealed the impact of the ionic strength on the thickness (via the absorbance) of a PLL/DNA film. Their results are showed on the figure 1.8. It is obvious that the layer thickness increase with the salt concentration, and that at too high concentration, a desorption occurs.

Salt type

At high ionic strength (higher than 0.1M), the ion type can impact the structure of the polyelectrolyte multilayer, since the ions are responsible for the screening of the charges along the chain. The interaction between polyelectrolytes and monovalent counterions were studied by Hofmeister. He divided the ions in two categories. The first one represents the structure makers ions, F^- or Na^+, for example, which have strong affinity with water molecules and are therefore protected by a water shell. These ions do not interact intensively with the polyelectrolytes of the solution. However, the second category of ions provokes a charge screening along the chains because their weaker interactions with water can be easily replaced by interactions with the polyelectrolyte. These structure breakers ions, such as I^- or Cs^+, are therefore the ones that influence the layer thickness. Nonetheless, this model states only for the monovalent ions, and an explanation

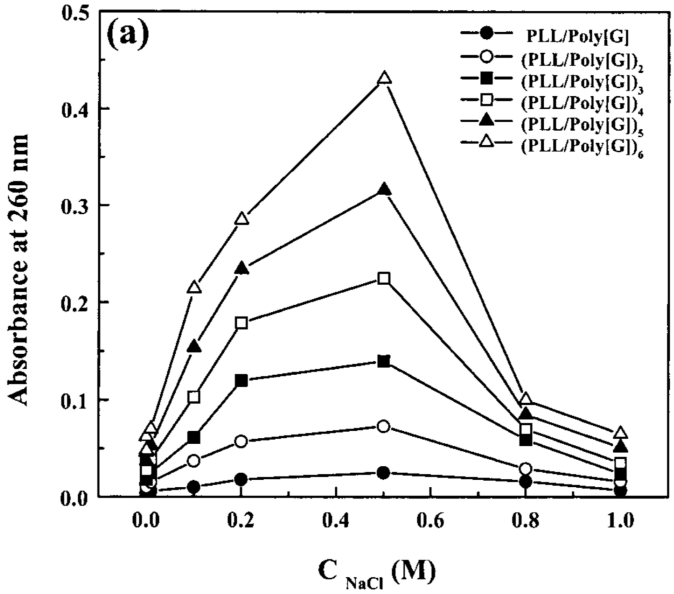

Figure 1.8: Absorbance values of individual PLL/DNA bilayers in the multilayered films plotted as a function of NaCl concentrations used for the film preparation. [31]

for monovalent-divalent interactions is already much more complicated. Moreover, a full understanding of the impact of the type of ions on the film building is not yet reached, given the huge number of ion-polymer interactions. [23][32][33]

Dipping solution pH

pH is an important parameter of the build-up of polyelectrolytes multilayer. It impacts the thickness of the film, its growth regime and its stability. It mostly affects the strength of the weak polyelectrolytes. Indeed, strong ones remain ionised on a large range of pH values, unlike weaker ones, for which even small pH change can influence the way the polyelectrolyte is charged. A weak polyanion needs a pH higher than its pKa in order to be negatively charged, while a weak polycation needs a pH lower than its pKa to be positively charged. By playing on the pH, the complementarity between the charges of the two polyelectrolytes can be adapted in order to have more or less interactions. As was explained on the section 1.3.3, less interactions lead to a thicker film when stronger ones induce thin layers.

Bieker *et al.* studied the influence of the pH on the PAA/PAH film construction. In figure 1.9, one can see five zones, with diverse growth law and layer thicknesses. The difference between the net charge of the polyelectrolytes, called the charge mismatch, is created by the pH changes, and is the reason why these five zones exist. In the first and the last regions, one of the two polymers is almost fully charged while the other bears few charges. The highly charged chains flatten on the surface, and the poorly charged ones form a thick layer in order to compensate the charges. The growth is linear in this zone. Zones II and IV correspond to a higher pH than zone I or lower than zone V, respectively. The poorly charged polymer carries more charges and the interdiffusion can occurs. The growth is exponential (see section 1.3.3). And finally, region III corresponds to two almost fully charged polymers, and therefore the layers are thin, with a linear growth. [20] [34] [35]

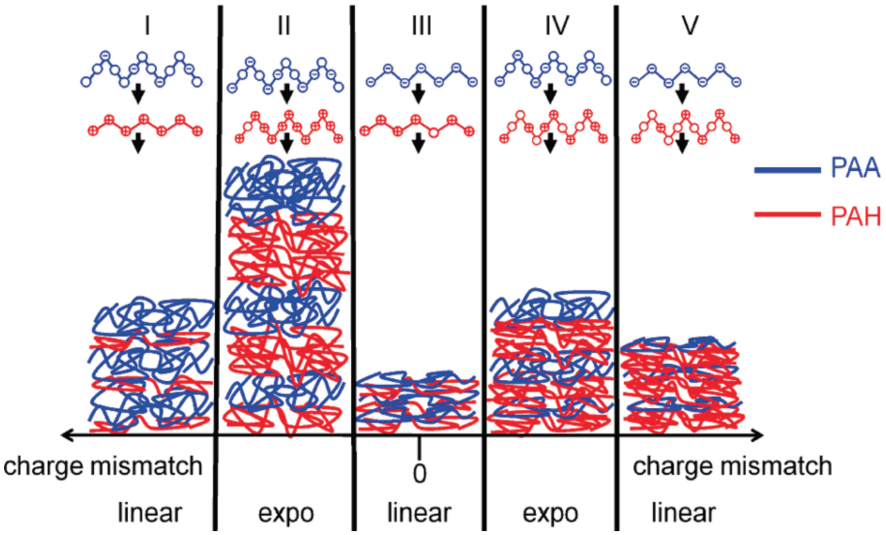

Figure 1.9: Growth behavior of PAA/PAH polyelectrolyte multilayer in dependence of charge mismatch, indicating regions with different growth laws, exponential vs linear, and sketching the film composition. [34]

Temperature

Temperature influences also the structure of a polyelectrolyte multilayer. With a temperature increase, polyelectrolytes become more coiled shaped. This shape is kept when the polymer adsorbs on the surface, making the layer thicker. A transition between the two growth regime can also appear, as Salomäki *et al.* showed with PAH/PSS multilayers (figure 1.10). They explained the transition by a swelling of the layers with the increase of the temperature, leading to more diffusion, and therefore, to more and more thick layers. [36]

Molecular weight

Although molecular weight is known to play a role in the multilayer build-up, this role is not yet fully understood. Lösche *et al.*, for example, showed a small effect on the thickness of PAH/PSS film from low to high molecular weight. But they also concluded that the role played by the M_w in the morphology, was minor in comparison to the ionic strength. [37] Nestler *et al.* studied the influence of M_w on PDADMAC/PSS multilayers. They concluded that below a certain threshold, decreasing PDADMAC or PSS molecular weight induces a change in the growth regime, and that the polyions impact the regime in opposite ways depending on the persistence length and the linear charge density. [38] Finally, Micciulla *et al.* showed that small chains are more subject to degradation than larger ones, on PSS/PDADMAC film, which modifies the architecture of the film. [39] Other studies have also been conducted, but a consensus of the influence of the molecular weight has still not been found, although it is recognized that it has a role to play in the growth of films.

Deposition time

The influence of deposition time on BPEI/MMT and BPEI/LAP films was studied by Yang *et al.* and their results are shown on figure 1.11. Increasing the dipping time leads

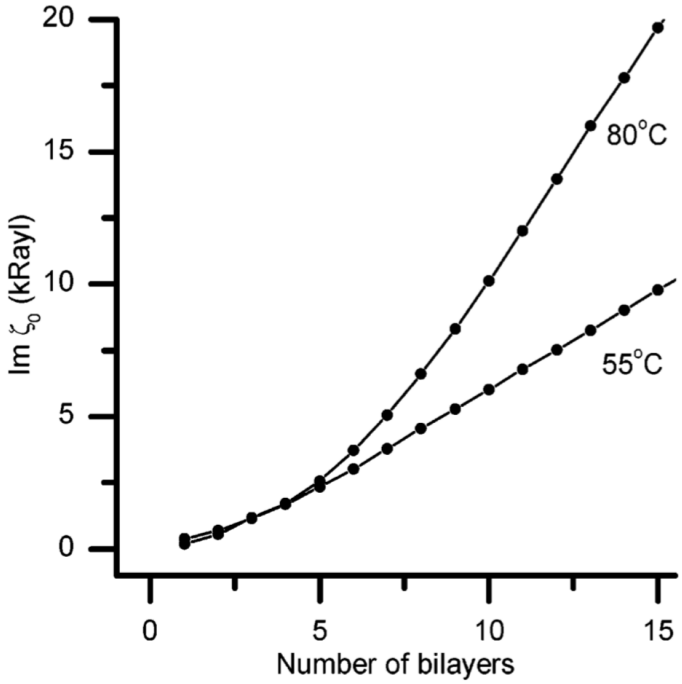

Figure 1.10: Imaginary part of the local acoustic impedance of a quartz crystal microbalance measurements of PSS/PAH multilayers deposition at two different temperatures (to describe the mass increment at the surface). [36]

to a thicker film, since more material is deposited. However, they obtained variations much larger with the BPEI/LAP couple than with the BPEI/MMT one. They explained this observation by the larger size of the *platelets* of MMT than those of LAP. Due to their size, MMT *platelets* can bridge defects of the previous layer and therefore, be a better support for the next layer. LAP, on the contrary, is not able to plug the holes and thus, when fewer MMT is deposited, fewer LAP adsorb leading to thinner film. To conclude, larger dipping time allows thicker polyelectrolyte multilayer but the impact of this parameter depends on the nature of the polyelectrolytes. [40]

1.3.5 Multilayer response to the environmental conditions

Water content

As water is an active component of the multilayer, the geometry of the film is different if it is kept in air or in water, and the phenomenon influences the internal stability and dynamics of the layers. Indeed, the polymers deposited form a highly hydrated structure, and changes in the environment water content influence the electrostatic forces between the layers. Moreover, water can also induce a larger mobility of the chains, and by swelling or shrinkage, an evolution of the layer thickness.

In their book, Gero Decher and Joseph B. Schlenoff justify the impact of the water content by the need of *waterbone species*. These species control the chemical potential and the osmotic pressure, establishing an equilibrium between the film and the environment (liquid or humidity). Studies support their theory: by the use of neutron reflectometry on PAH/PSS multilayer, Schmitt *et al.* demonstrated that PSS was surrounded by four molecules of water, at ambient conditions. The water content determined was of 27%

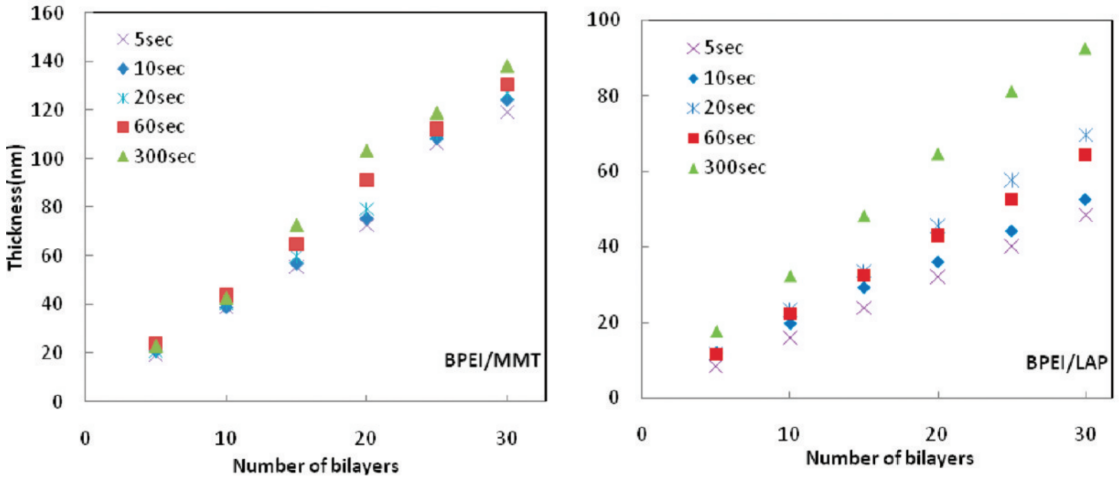

Figure 1.11: Ellipsometry measurements of film thickness as a function of bilayers deposited for LbL assemblies made with varying deposition times. BPEI/MMT film (left), and BPEI/LAP one (right). [40]

inside the multilayer. [41] Five years later, Lösche *et al.* showed a swelling of 42% volume fraction when the film was fully hydrated, and the presence of six water molecules linked to the PSS, while PAH carried only one. [37] Others examples, including with other building blocks than PAH/PSS, exist in the literature and also agree with their theory. [42]

As swelling is due to hydration of the film, leading to an increase in the thickness, dehydratation provokes shrinkage and leads to thinner film. However, it is important to note that, due to the steric hindrance, 40% of the volume of the water released is not filled by the macromolecules, creating voids in the structure. [37]

pH

Geometry of the film is also influenced by the pH of the surrounding environment. In their work, Chia *et al.* studied the behavior of a PAH/PAA multilayer upon pH changes. At high pH, the carboxylate groups of PAA are protonated, and the links between NH_3^+ and COO^- are therefore broken. The system is swollen. When the pH decreases, a transition occurs due to the deprotonation of the carboxylate groups: links between the two polyelectrolytes can be made again, and the film is thinner (see figure 1.12). Upon drying, the system at high pH will lead to a thicker film than the one at low pH. Indeed, at low pH, the chains have a higher mobility and can thus fill the space occupied by the water when the multilayer is wet. At high pH these spaces become air pockets when the system is dried. It is therefore important to know how the system will behave with the pH conditions, as it influences its thickness, but also its porosity.

1.3.6 Membrane templated technique as assembly method

The use of nanotubes became more and more widespread, thanks to the easily tunable size, length, composition, and thickness. One common, simple and versatile way to produce nanotubes, and control their characteristics, is using nanoporous membranes as support for the LbL growth. Polymers adsorb on the walls of the pores of the membrane, forming tubular structures. Nanotubes are then released by the dissolution of the membrane. This method, called membrane templating, was developed twenty years ago by Martin *et al.*

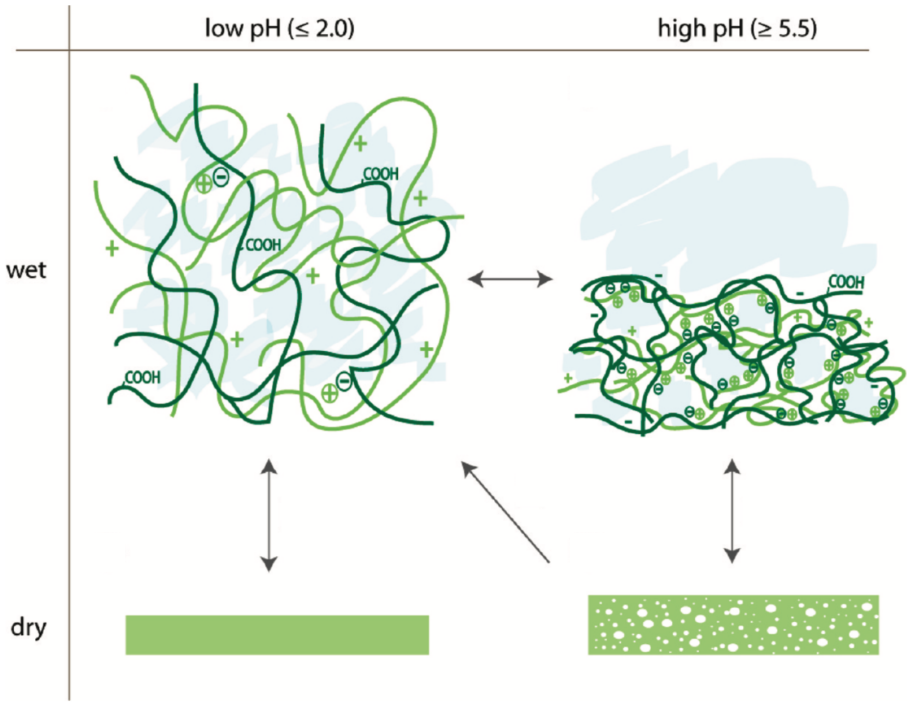

Figure 1.12: (A, B) Molecular arrangements of the polymers in a PAH/PAA multilayer film in high- and low-pH solutions and (C, D) morphology of the films upon drying [43].

[44]. This section first clarifies what is the membrane and how it is produced, and then, the main differences between the LbL deposition on flat surface (what was explained until now) and inside a membrane are highlighted. [20]

Nanoporous membrane fabrication

The most used membranes for the synthesis of nanotubes are anodic aluminum oxide (AAO) or track etched polycarbonate (PC), polyethylene terephthalate (PET) or polyimide (PI) membranes. As indicated by its name, AAO membrane are produced from an alumina film that undergoes a two-step anodisation. The first anodisation leads to random pores, organized in depth. Thanks to this organization, the etching of the top aluminium oxide leads to a surface with ordered templates, helping the second anodisation in the construction of a well organized honeycomb-like structure (figure 1.13).

The size of the pores and the density can be tuned by the conditions of the anodisation process, while the anodization time controls the thickness of the template. Note that higher the density of the pores, smaller their size, and inversely. Commercially available dimensions are: 10 to 200 µm for the template thickness; 10 to 150 nm for the pore diameter; and 10^9-10^{11} pores $\cdot$ cm^{-2} for the pore density. [46] [47]

Figure 1.14 represents how polycarbonate thin films are transformed in porous membranes. First, linear damage tracks are produced. This damaged chemical bonds come from the bombardment of the film by heavy ions, accelerated in a cyclotron. Then, the film goes through etching bath, allowing to remove the degraded polymer, to finally have well-defined pores. Etching solution concentration, temperature, pH and time influence the diameter of the pores, that can go from 10 nm to 10 µm. The porosity usually ranges

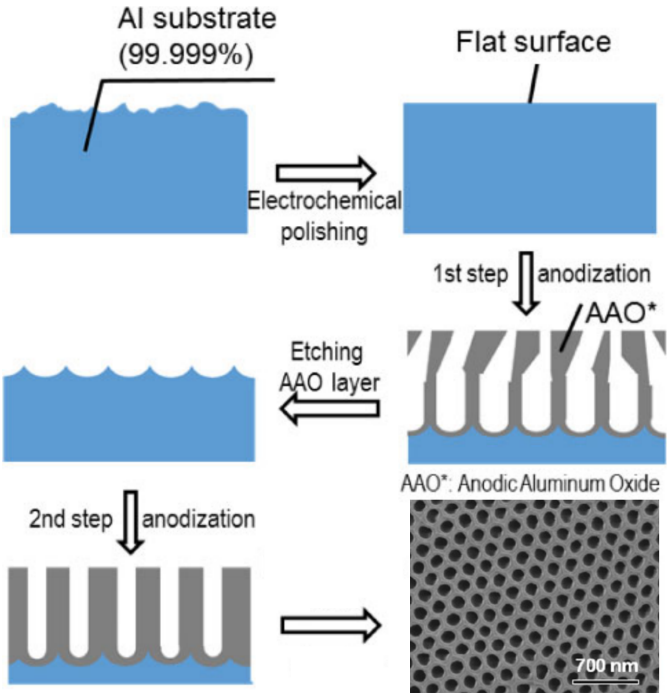

Figure 1.13: AAO fabrication process. Adaptation of images from [45] (schema) and W. Lee and K. Nielsch (SEM image)

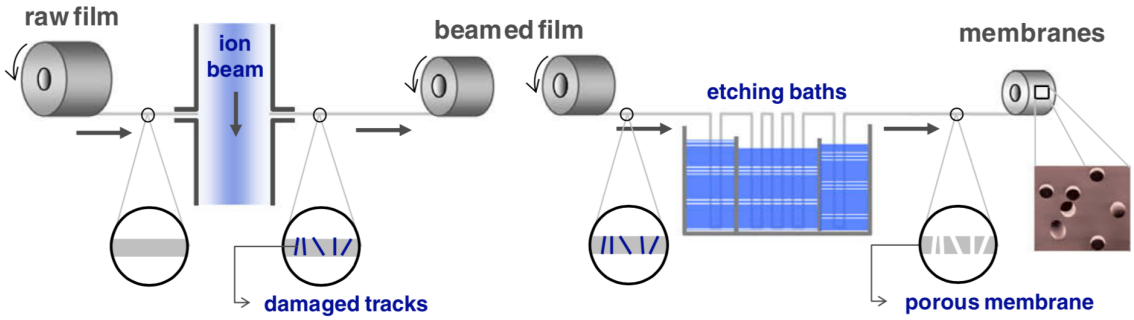

Figure 1.14: Schematic of roll stock track etched membrane manufacturing. [48]

between 10^5 and $6 \cdot 10^8$ pores $\cdot$ cm^{-2}, and the template thickness is between 10 to 25 µm. Pore size and density of track-etched membranes are not related, as their are for AAO templates. [48]

AAO and PC are the most commonly used membranes. Although the pores are regularly distributed in AAO and not in PC membranes, the last ones are generally preferred. Indeed, it is easier to dissolve the polycarbonate, with a large range of solvants, than to dissolve the alumina, which requires extreme pH values.

Membrane templated LbL

As was already mentioned, membrane templated LbL is a common method to produce nanotubes, since the size, the outer and inner diameter and the composition of the tubular structure are easy to control. The technique is the same as the LbL deposition on flat

surfaces, except that the substrate is the pore wall of the membrane. This membrane is therefore dipped into successive polyanion-polycation baths, depositing concentric layers on top of each other. The template is then dissolved in order to collect the tubes (figure 1.15).

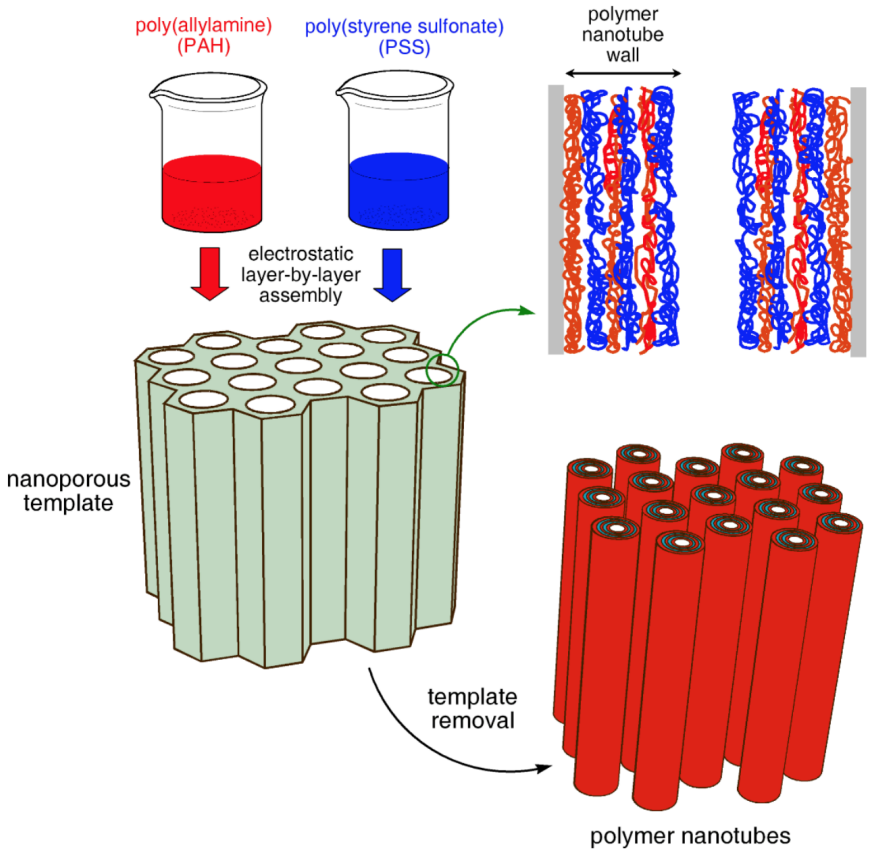

Figure 1.15: Schematic representation of membrane templated LbL technique [49]

1.3.7 Nanotubes growth mechanism

Even though the principles described in the sections 1.3.1 to 1.3.5 remain true, the membrane templated LbL is not exactly as easy as the LbL on flat surfaces. The main difference comes from the nanosize of the pores. In order to adsorb, the polymer has to diffuse into the pore. Its diameter thus influences the growth of the LbL deposition. Indeed, it has been observed by Alem *et al.* that the layers are thicker than on flat surfaces. The implication of the molecular weight and the ionic strength on this increase were discarded, while it appears that the diameter of the pores of the membrane is the key parameter to explain the difference between the deposition on the two substrates. [50]

Roy *et al.* showed the existence of two growth regimes, one rapid and one with reduced kinetics. In the first regime, the diffusion through the pore does not limit the deposition, which is linear and comparable to the one on flat surface. In the second regime, however, the polyelectrolytes chains yet adsorbed on the surface almost fill the pore. Chains across the pore interconnect, and a dense gel is formed. The diffusion through the pore is now the controlling parameter. The more polyelectrolyte deposited, the more interconnections, and the slower the diffusion. One could conclude that nanowires are so formed, but upon

drying, the polymers shrink, leading to the formation of nanotubes, as it is showed in figure 1.16. The transition between the two regimes occurs when the interconnections across the pore are first formed, but it can be reached even after one bilayer deposition, depending on the pore diameter and probably on the size of the polyelectrolyte chains. [51]

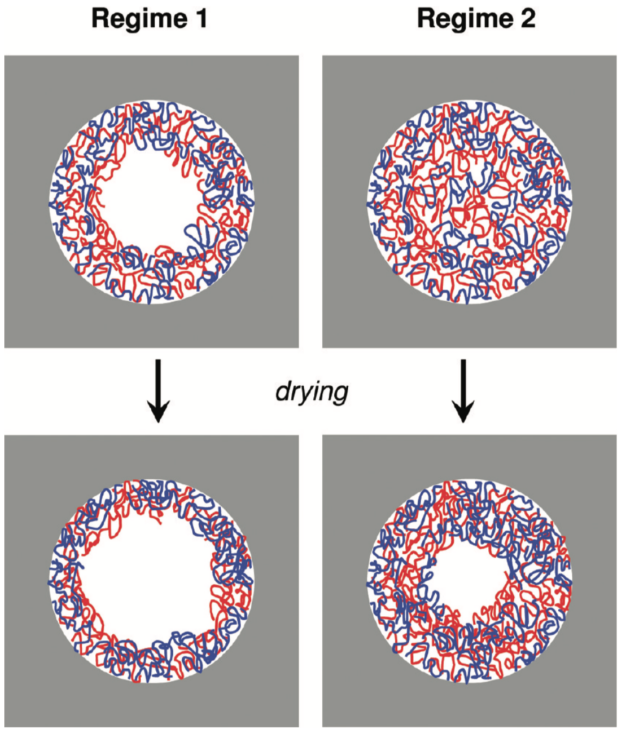

Figure 1.16: Schematic representation of polyelectrolyte multilayer structures in nanopores corresponding to regimes 1 and 2 before and after drying. [51]

As the diffusion makes the membrane templated LbL technique slower than the LbL on flat surfaces, dipping time must be increased. PAH/PSS nanotubes dipping time optimization is a topic of the research work of this master thesis, and is presented in section 3.1.

Another parameter that must be adjusted compared to the LbL on flat surfaces, is the ionic strength. Indeed, ionic strength modifies the shape of the polyelectrolytes, as explained in section 1.3.4. If the pore diameter is very small, it is necessary to reduce the size of the polyelectrolyte by adding salts, to enter into the pore and adsorb on the wall. However, a too high salt concentration can provoke a neutralization of the chains, and thus prevent their deposition. Moreover, the chain could precipitate in the dipping solution, or create clusters in the pores, and block them. Therefore, the salt concentration needs to be adjusted, neither too high nor too low, to obtain well shaped nanotubes.

1.4 Nanopapers of nanotubes

Filamentous membranes, usually built by electrospinning, are widely used for biomedical applications such as tissue engineering, sensors, enzyme-immobilization and filtration system [52]. Indeed, they offer a porous, high surface-area to volume ratio system, allowing to reduce the amount of material used while providing sufficient surface available to perform the reactions wanted. Layer-by-Layer deposited nanotubes, in addition, enables the use of a wide range of materials and a tunable surface chemistry. Zhang *et al.* proposed a way to combine the two methods in order to build filamentous membranes from a filtration of nanotubes in suspension on a porous membrane. [2]

The group studied different mat textures, by playing on the rigidity of the tubes. Indeed, the morphology of the mat is affected by deformations of the tubes such as flattening, twisting and scrolling, and their occurrence depends on the tubes rigidity. Figure 1.17 shows SEM images of nanotubes (column a) and AFM topography images of the mats built from these tubes (columns b and c) under three categories of nanotubes building conditions, influencing their rigidity. On the right images of the figure, the categories are referenced. The tubes of category A were built at the "natural" pH of the polyelectrolytes (PAH/PSS). At this pH, the polyelectrolytes are fully charged and therefore the layers are thin (section 1.3.4). Second category, B, represents mats produced by the filtration of nanotubes built at a pH of 7.0. In these conditions, the PSS is still fully charged, but the PAH lose charge density. The layers are thus thicker. Finally, the addition of salt leads to condition C. As explained in section 1.3.4, the increase of ionic strength allows the construction of thicker layers. The amount of bilayers and the pore diameter of the template (so the outer diameter of the tubes) are referenced in the images of the column c.

The study showed that coarser texture are obtained with larger outer diameter of the tubes. Moreover, mats are more rough and their pores larger (three first images, of category A). The deformation of the tubes (flattening, twisting and scrolling) in suspension are highlighted in images of column A. These effects are also present in the mats, influencing the opening of the network. For example, mats grown under condition C show an open network with straight tubular species, while under conditions A the texture is less easy to characterize. Images also provide the information that the diameter of the tubes are smaller in the mats than in suspension, probably due to the stronger forces that the tubes undergo when they are collected to form a mat.

The group also studied the influence of the density of tubes on the paper's texture. They showed that under 10^9 nanotubes $\cdot\,\mathrm{cm}^{-2}$ mats were not continuous. Indeed, they observed nanopapers with nanotubes tagged with a fluorescent marker thanks to fluorescence microscopy. They saw big clusters separated by gaps (figure 1.18). However, even when the mat was continuous (i.e. with a density of tubes larger than 10^9 cm^{-2}), the presence of the clusters was still noticeable. They concluded that nanotubes accumulate in clusters, and the gaps between them are progressively filled until a continuous mat is formed.

Zhang *et al.* also showed that nanopapers can be functionalized if one of the building block is active, or by post-functionalization of the mat, or even by the superposition of layers containing different types of nanotubes.

By developing such a new kind of filamentous membrane, the group gave a tool to de-

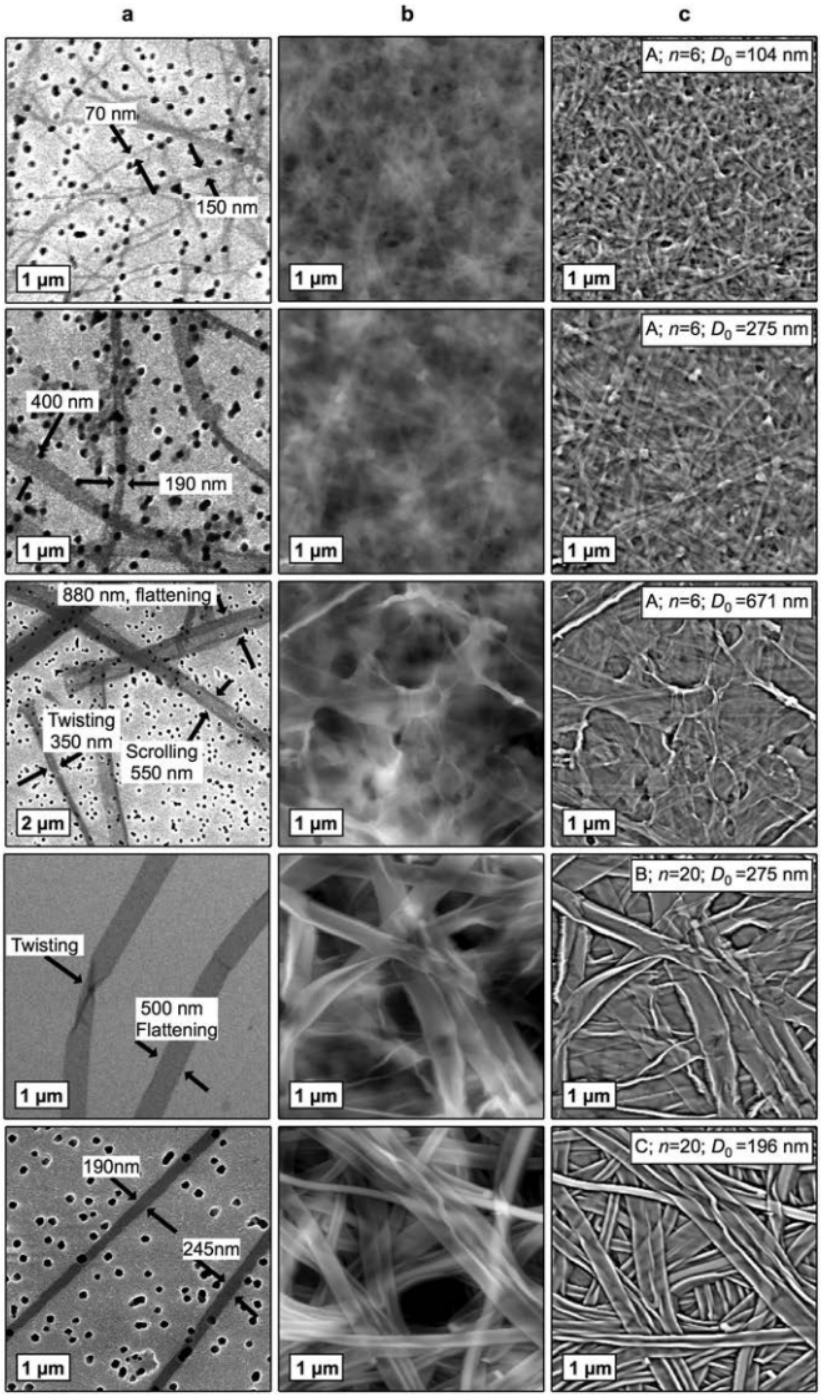

Figure 1.17: SEM images of PAH/PSS nanotubes grown under different conditions (description in column c) and collected on filtration membranes (column a), and AFM topography images of the nanopapers based on these nanotubes (columns b and c). The grey colour levels span 450 nm in column b; column c displays the high-pass flattened images of column b, revealing the nanotubes located deeper in the nanopaper. The growth conditions, A, B or C, are indicated for each row of images in column c; D_0 is the measured pore diameter of the templating membranes and n the number of LbL cycles. A few measured diameters are indicated, as well as typical modes of deformation of the nanotubes. [2]

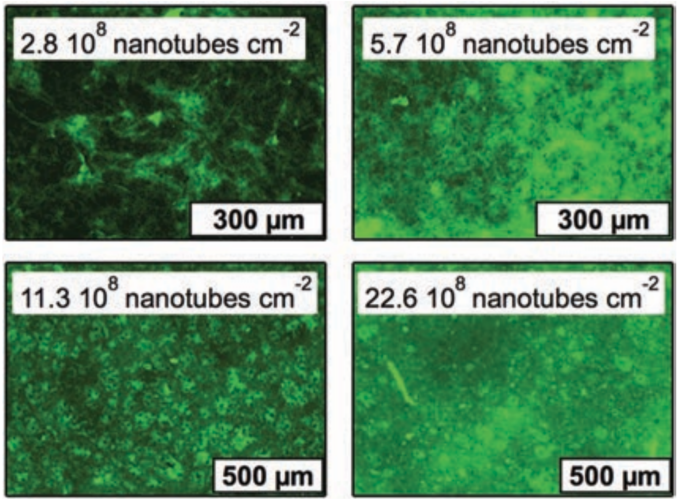

Figure 1.18: Epifluorescence microscopy images of nanopapers made of FITC- tagged $(PAH/PSS)_6$ nanotubes grown under conditions A in membranes of 300 nm nominal pore diameter. The approximate amount of nanotubes collected per unit area is indicated in the images. [2]

sign new technologies such as the one studied in this work: medical patches containing bacteria.

Chapter 2

Materials and methods

2.1 Materials

2.1.1 Polymers

Poly(sodium-p-styrenesulfonate) (PSS) of average molecular weight 70 kDa was purchased from Acros organics. Poly(allylamine hydrochloride) (PAH) of molecular weight between 120 and 200 kDa was purchased from Alfa Aesar. Poly(ethyleneimine) (PEI) of average molecular weight 750 kDa was purchased from Aldrich. Glycol Chitosan (gCHT) of polymerization degree ≥ 400 and Sodium Alginate (ALG) were purchased from Sigma-Aldrich. Their chemical structures are shown in figure 2.1.

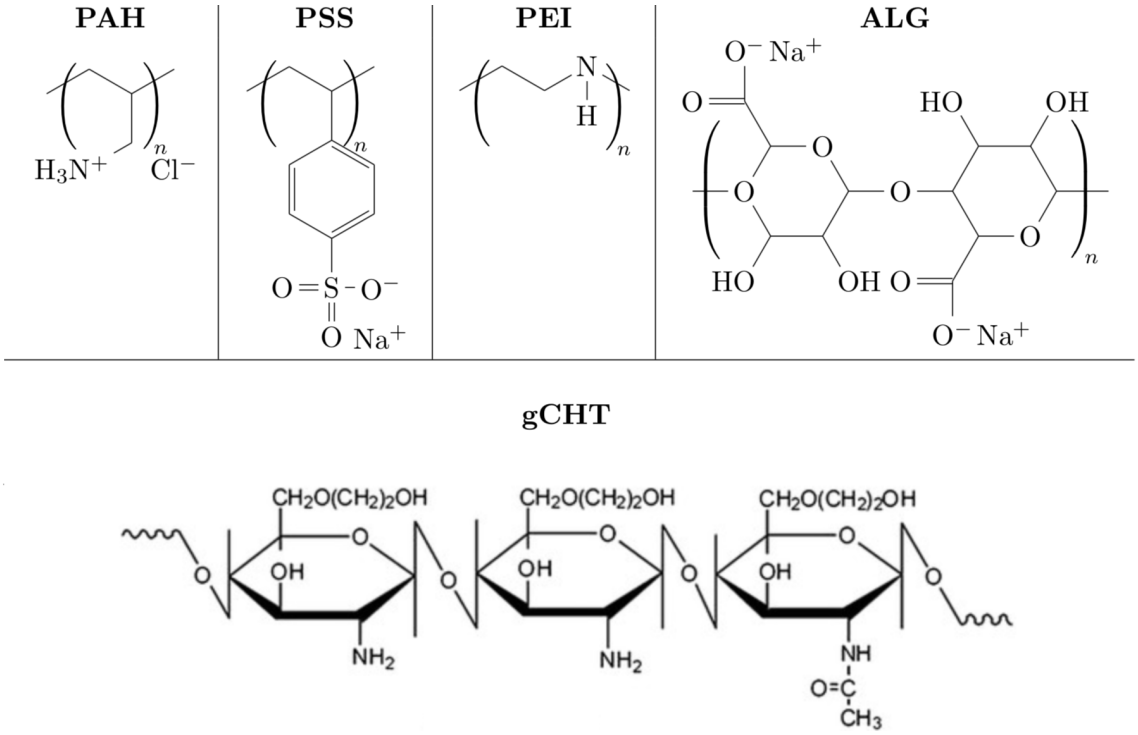

Figure 2.1: Chemical structure of polyelectrolytes PAH, PSS, gCHT and ALG, and polymer PEI.

2.1.2 Substrate

Track-etched membranes were purchased from It4ip (`http://www.it4ip.be`, Louvain-la-Neuve). Characteristic of polycarbonate (PC), polyester (PET) and polyimide (PI) membranes are summarized in table 2.1. Membranes were cut in 6x6 cm^2 or 10x10 cm^2 squares to use is as template for the deposition of the tubes. To serve as a filter, the membranes were cut in disks of two cm diameter (section 2.2.1).

Material	**Pore diameter** [µm]	**Average pore density** [pores/cm^{-2}]	**Thickness** [µm]
PC	0.3	10^8	25
PC	0.8	$4 \cdot 10^7$	24
PET hydrophilic	0.8	$4 \cdot 10^7$	22
PI hydrophilic	0.2	$5 \cdot 10^8$	25

Table 2.1: Characteristics of membranes purchased from It4ip.

Topsil supplied the silicon wafers used for the assembly on flat surfaces. The crystal orientation was [1-0-0], and they were n-doped with Phosphorus. They had a polished top surface and an alkaline etched back surface. The thickness was 500 to 550 µm.

2.1.3 Solvent, fixative, adjuvent, water and latex particles

Glutaraldehyde ($OHC(CH_2)_3CHO$) in solution (8% in H_2O) from Sigma-Aldrich was used as fixative. To dissolve the PC membrane, dichloromethane HiPerSolv CHROMANORM for HPLC (CH_2Cl_2) was purchased from VWR International. As explained in section 2.2.1, an adjuvent was added when the tube were transfered to water. It was Dextran (from Leuconosctoc spp., M_r: 70 kDa) supplied by Sigma-Aldrich. The water used in all experiments was purified by a millipore system (Milli-Q water of 18 MΩcm resistivity). Finally, latex particles in aqueous suspension used to model the bacteria were also purchased from Sigma-Aldrich. They were made of carboxylate-modified polystyrene and tagged with yellow-green fluorescent ($\lambda_{ex} \sim 470$nm, $\lambda_{em} \sim 505$nm). Their mean diameter was one µm, as shown on figure 2.2.

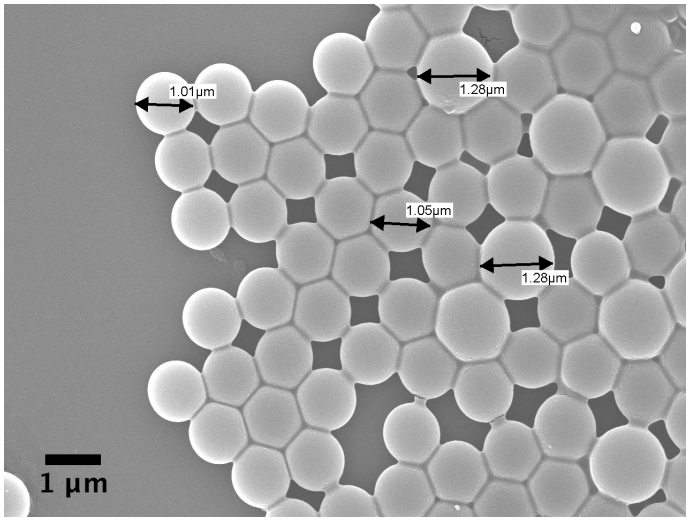

Figure 2.2: SEM image of the latex particles, with measurements of their size

2.2 Methods

2.2.1 Nanotubes

Synthesis

Polycarbonate membrane was dipped in polyanion-polycation solutions alternately (step (a), (b) and (c) of figure 2.3). Solutions were prepared just before the assembly. The concentration of polymer was fixed at 1 mg/mL, and the ionic strength at 0.5 M (for polyelectrolytes PAH, PSS and PEI) or 0.15 M (for ALG and gCHT) in water. The pH of the solutions was controlled with a pH-meter and was adjusted with HCl and NaOH to be between 6.5 and 7. Rinsing solution had the same ionic strength as the one of the polyelectrolytes solutions used to built the nanotubes: 0.5 M for nanotubes of PAH and PSS, and 0.15 M for nanotubes of ALG and gCHT. Polyanion was deposited first in order to facilitate the release of the tubes from the polycarbonate membrane. The membrane stayed 5, 10 or 15 minutes in the polyelectrolyte solution and was dipped in two rinsing baths for two minutes between each deposition. n-Bilayers were obtained by repeating the polyanion-$(\text{rince})_2$-polycation-$(\text{rince})_2$ cycle n times. Every three bilayers, the membrane was decrusted with a cotton swab in Milli-Q water, to avoid the building of a film on the top and the bottom of the membrane and the encrusting of the pores (step (d)). Rinse solutions were renewed after three dipping of the membrane in it.

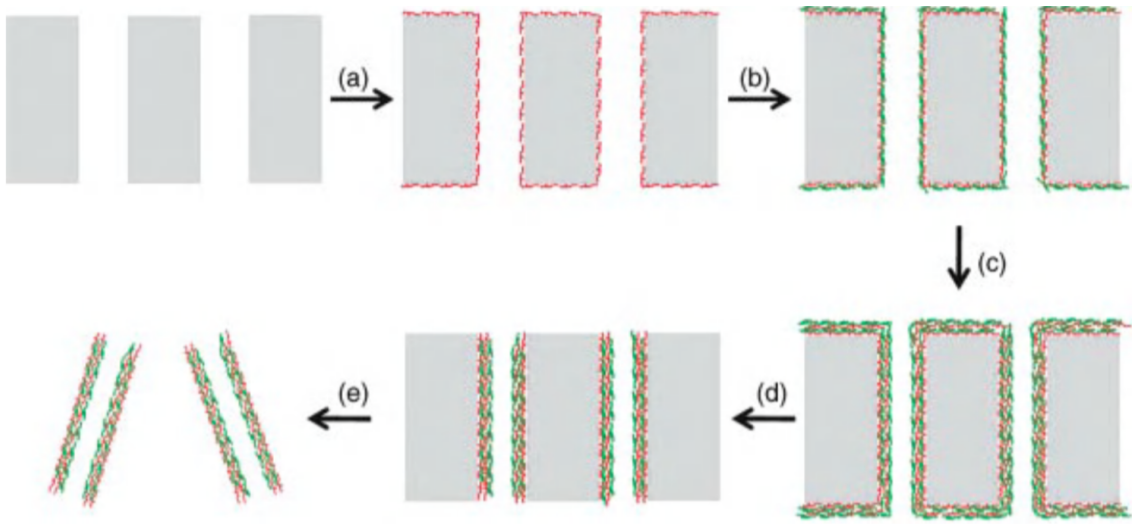

Figure 2.3: Scheme of one cycle of the assembly of polyelectrolytes multilayers inside nanopores [53].

Transfer in water

Nanotubes were released from the polycarbonate membrane by its dissolution in the dichloromethane solvent (CH_2Cl_2) (step (e) of figure 2.3). The adjuvant-assisted filtration technique developed by Saghazadeh *et al.* [23] was used (fig. 2.4): Dextran was added (0.042 g/cm^2 of polycarbonate membrane, or 10^8 nanotubes) in order to avoid the agglomeration of the tubes further in the process. To be sure of a complete dissolution of the membrane, the solution of CH_2Cl_2 with the tubes was sonicated. It was then filtrated under vacuum through the system shown in fig.2.5. Polyimide membrane with pore diameter of 0.2 µm was used as filter. Figure 2.4 represent the steps of the filtration: 300 µg

of dextran was placed on the PI membrane, followed by the filtration of CH_2Cl_2 to make a porous compact cake. Tubes and dextran suspension in dichloromethane was then filtrated through this system. Nanotubes were therefore trapped in dextran. Additional dichloromethane was filtrated through the pellet formed, to completely dissolve the PC.

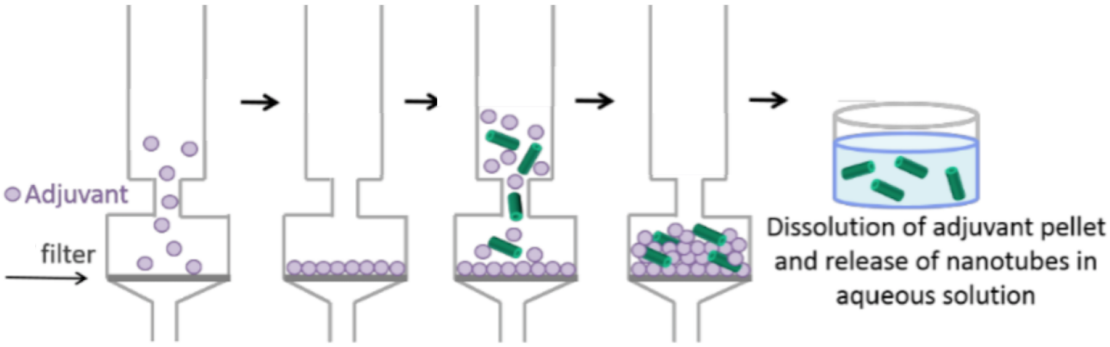

Figure 2.4: Schematic representation of nanotube collection by the adjuvant-assisted filtration method. Figure adapted from [23].

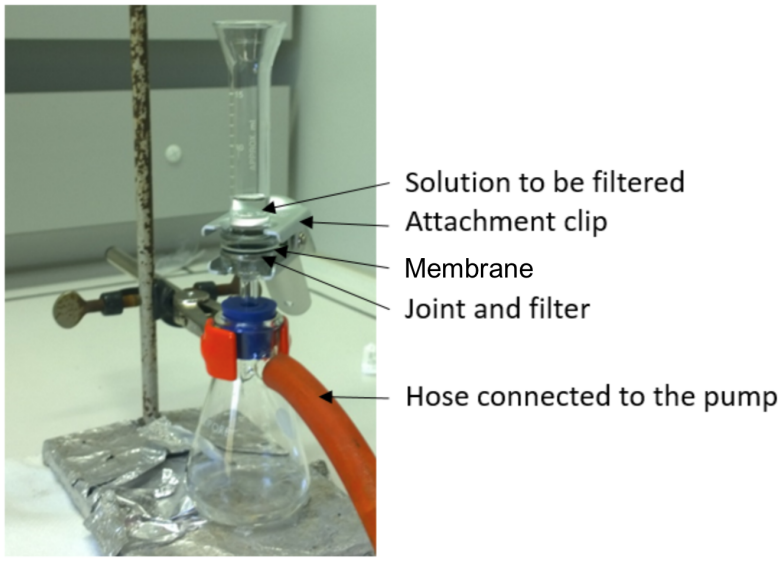

Figure 2.5: Filtration system used to release the nanotubes from the polycarbonate membrane. Figure adapted from [54].

Powder of dextran and nanotubes was collected and dried overnight under vacuum in order to remove all the dichloromethane. Finally, saline solution (0.15 M) was added to dissolve the dextran and suspend the tubes. Solution was shaken to accelerate the dissolution.

2.2.2 Mats fabrication

Without particles

The same filtering system (showed on fig. 2.5) was used to build the mats. Tube suspension in water (for SEM observation) or saline solution were filtered on a PET membrane (pore diameter 0.8 µm). Mat was thus formed because of the nanotubes accumulation on the PET membrane. The whole was kept in saline solution (0.15 M).

With particles

Following the same methodology, three mats were filtrated on top of each other, as shown in fig. 2.6. The layer of the middle contained latex particles. Indeed, $400 \cdot 10^6$ particles for $2.5 \cdot 10^9$ nanotubes (5x5 cm^2 of polycarbonate membrane) were added in tube suspension before filtration. The 3-layered paper was kept in saline solution (0.15 M).

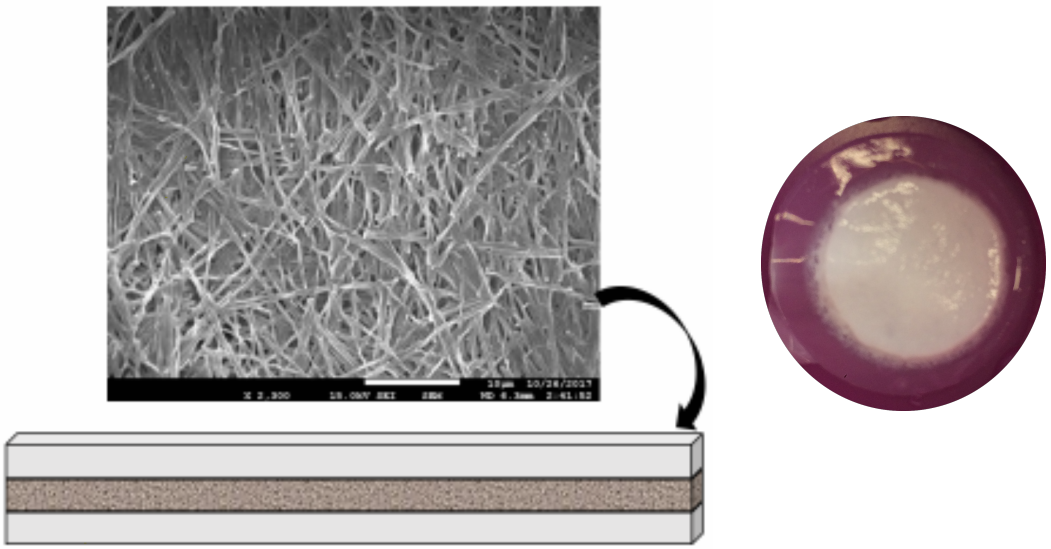

Figure 2.6: Left: Structure of the paper: 3 films of PSS/PAH nanotubes on the top of each other. The one in the middle contains particles. Typical SEM image of mat. Right: photo of a mat (in Falcon tube plug).

Fixation

To ensure better mechanical properties for the microtomy (section 2.3.1), papers were fixed with a solution of glutaraldehyde 2% in NaCl 0.15 M. Samples were put in contact of the solution three times: first for 30 minutes at 30°C, then 15 minutes at 30°C and finally one hour at ambient temperature. Three rinses were then performed (10 min each, in NaCl 0.15 M, at ambient temperature).

Adhesion and cohesion

Two techniques were developed to improve the stability of the paper:

- To make the mat adhesion on the support better, PET membrane was coated with PEI or PEI/PSS (all 1 mg/mL in NaCl 0.5 M) before the filtration of the tubes suspended in water.
- Cohesion of the paper was increased with a LbL deposition of a $(PAH/PSS)_6$ film on top of the structure. PAH was the first deposited polyelectrolyte. The other technique tested was the complexation of oppositely charged polyelectrolytes also on top of the 3-layered mat.

2.2.3 Multilayer assembly of gCHT and ALG on flat surface

Before use, silicon wafers were cleaned with piranha solution (H_2SO_4 (98%)/H_2O_2 (32%), 1/1 v/v) for 20 minutes. The adherence of the film on the surface was increased by the dipping of the wafers in PEI solution (1 mg/mL in NaCl 0.5 M) for five minutes, followed by two rinsing in saline solution (NaCl 0.5 M, two minutes). Same process of multilayer construction as the one described in section 2.2.1 was followed: the wafers were dipped in polyelectrolyte solution for five minutes, and rinsed in a saline solution (two minutes) two times between each polyelectrolyte bath. After the repetition of the cycle n times, wafers were carefully dipped in Milli-Q water to remove the salt without destroying the multilayer assembly. They were then dried and finally stocked in Fluoroware Single Wafer boxes in order to perform ellipsometry analysis (section 2.3.2).

2.3 Characterization techniques

2.3.1 Microscopy

Microtomy and optical microscopy

One mm slices of papers were obtained by microtomy. The technique is based on the rotation of a blade (diamond for this work). The blade is first below the sample, then it goes up and therefore cut the sample. It is then moved back and below and the cut can be collected. Finally, the blade goes forward and therefore is again located below the sample. The cycle can start another time to produce a new cut.[55] The device used was an ultra microtome Reichert, with a cryogenisation chamber. As the paper was soft, thick, fragile and heterogeneous, its cutting was not easy to perform, even at -70°C. To facilitate it, the sample was surrounded by a drop of water: the paper was inserted in the pliers of the microtome, and water was carefully put in contact with the structure. Because of the low temperature, the water directly froze, and the paper was therefore trapped in ice: figure 2.7. Cuts were observed by optical microscopy, with an Olympus AX70/Provis.

Figure 2.7: Entrapping of the sample in water for microtomy.

Scanning Electron Microscopy

Morphology of nanotubes and mats was analyzed by scanning electron microscopy. The surface of the samples was scanned with a focused beam of electrons. Its morphology could be determined thanks to the interactions between the electrons and the matter. [56] In order to observe the tubes and the mats by scanning electron microscopy, saline solution in which they were kept was replaced by Milli-Q water. For nanotubes, a drop of the suspension in water was deposited on a gold-coated PET membrane and the samples were dried. Before imaging them, the mats were metallized with a 20 nm layer of gold. The metallizer was a Cressington 208HR High Resolution Sputter Coater, while the SEM was a JEOL 7600F. Acceleration voltage was fixed at five kV, and working distance at height mm.

Fluorescence microscopy

The fluorescence of latex particle into the mat or in the supernatant of the solution in which the mats were kept was analyzed by means of epifluorescence microscopy. It is based on the capacity of some materials (the latex particles here) to absorb high energy photons and emit light after that. Thanks to microscopy, this emitted light is detected and an image is formed. [57] For this work, an Olympus IX71 inverted microscope equipped with a green filter set was used to see the samples and the supernatant in which the mats were kept.

Confocal

Samples placed between two glass slides were characterized by confocal microscopy with a Zeiss LSM 710 microscope. Thanks to a spatial pinhole, out-of-focus light of the microscope is blocked when the image is formed. It allows to capture multiple 2D images at different depth and then 3D images can be reconstructed. [58] Green filter was used to see the particles, as well as a x25 objective. Stack of images were acquired and the 3D-reconstruction was performed with the software ImageJ. Separation between the plans was the smallest possible, i.e. five µm.

Atomic Force Microscopy

Atomic force microscopy in tapping mode was used to characterize the roughness of the multilayers assembled on flat surfaces. The AFM technique is based on the scan of a surface with a probe. Interactions between sample atoms and the probe are detected. As they reflect the topology of the surface, an image can be formed by the analysis of these interactions. In tapping mode, the probe oscillate at its resonance frequency, with a determined amplitude. When it interacts with the surface (Van der Waals and electrostatic forces, dipole-dipole interactions, etc.), the oscillation frequency and the amplitude change. This variation of amplitude is the parameter used to form the image. [59] The films were imaged without any further preparation with a Bruker Icon Dimension. Probes used were PPP-NCHR-50 type from Nanosensors. Their resonance frequency and force constant were about 300 kHz and 40 N/m respectively. Images were then treated with ImageJ.

2.3.2 Ellipsometry

Ellipsometry was used to determine the thickness of the film built on flat surface. The very sensitive and accurate technique is based on the influence of the sample on the

polirized light emitted by the ellipsometer. Collimated and polarised light is sent toward the sample. When it reaches the surface, a part of the beam is absorbed, while the other part is reflected. The planar and polarised wave becomes an elliptical wave. The state of polarisation is therefore changed, depending on the surface nature. A detector receives the reflected light, and measurements of ellipsometric angles are done: the amplitude ratio Ψ and the phase shift Δ. These angles are representative of the ellipticity of the reflected light, and depend on the thickness and the reflection angle of the surface. [60] The ellipsometer used was a Accurion EP3+ ellipsometer. The wavelength of the laser was 658 nm. To determine the film thickness from the ellipsometric angles, the Accurion software with $n - k$ fix model was used ($n = 1.5$, $k = 0$). The thickness of the SiO_2 was subtracted from the measurements, after processing ellipsometry on a Si wafer as reference (a SiO_2 layer is present on top of the Si crystal).

2.3.3 Ultraviolet–visible spectroscopy

Supernatant of the mats was qualitatively analyzed through UV-spectroscopy. The aim was to see if there was decomposition and qualify in which conditions there was. The technique is based on the absorbance of the light by the sample. Depending on the nature of the sample, it will absorb light at particular wavelengths. The spectra calculated is the function between the intensity of the light absorbed and the wavelength of the light. [61] Analysis were performed between 400 and 800 nm of wavelength with a Varian Cary 50 UV-Visible Spectrophotometer. Software Varian Cary WinUV was used to get the data, and treatment of this data was done with Matlab.

2.3.4 Porometry measurements

The growth of the multilayer in the pores of the membrane was quantified thanks to gas-flow porometry measurement of It4ip. 0.137 cm^2 sections of PC membranes containing the nanotubes were analyzed at ambient temperature, after air-drying. The flowmeter used was a GMF Pro Gas Flowmeter. Air was sent upstream the sample with a pressure of 0.7 bar, and the gas flow was measured downstream (mL/min). From the lecture of the porometer, average nanopore diameter can be determined thanks to:

- the Knudsen diffusion:

$$J_{diff} = \frac{4}{3}\frac{d}{l}\frac{(P_{up} - P_{down})}{\sqrt{2\pi MRT}} \tag{2.1}$$

- the viscous flow (Hagen-Poiseuille):

$$J_{visc} = \frac{d^2}{l}\frac{(P_{up}^2 - P_{down}^2)}{64\mu RT} \tag{2.2}$$

where d is the pore diameter (m), l the thickness of the PC membrane (m), P_{up} and P_{down} the pressure upstream and downstream from the sample (Pa), M the gas molar mass (kg/mol), μ the dynamic viscosity of the gas (kg/ms), R the ideal gas constant (J/Kmol) and T the gas temperature (K).

Φ is the total volume flow rate (m^3/s) and can be determined by 2.1 and 2.2:

$$\Phi = (SP)\frac{RT}{P_{atm}}(J_{diff} + J_{visc}) \tag{2.3}$$

with S the effective section area of the membrane (m^2), P_{atm} the atmospheric pressure (Pa) and $P = N\frac{\pi d^2}{4}$ the transparency of the membrane (N is the pore density (m^{-2})).

Finally, the wall thickness t (m) of the tubes was calculated by:

$$t = \frac{d_i - d}{2} \tag{2.4}$$

where d_i is the initial pore diameter. [51]

Chapter 3

Results and discussion

3.1 Tube fabrication process optimization

The first step of this work aimed at optimizing the fabrication process of the nanotubes. PSS/PAH nanotubes were built into a PC membrane, at pH $\in [6.5, 7]$. At this pH, PSS is fully charged, while PAH is not. Resulting tubes are therefore thicker than if they were assembled at pH 4.0 for the PAH and 5.3 for the PSS, their "natural" pH, for which they are fully charged (see section 1.4).

Dipping time and amount of bilayers are two parameters of the fabrication process that influence the nanotube morphology. They also have a huge impact on the cost of the fabrication. Indeed, the assembly of 9-bilayer nanotubes with 15 minutes dipping time takes 6h30. It was therefore tried to reduce the time needed while keeping well-shaped tubes. Nanotubes were assembled with 3-6-9 bilayers (after three bilayers a decrusting step was performed) and the dipping time was fixed at 5-10-15 minutes. Tubes dispersed in water were analyzed by SEM as well as in mats. Porometry measurements provided the thickness of the walls of the tubes.

3.1.1 Integrity of tubes in water

The nanotubes were dispersed in water after the dissolution of the polycarbonate membrane, and a drop of the suspension was left to evaporate on a gold-coated PET membrane. After evaporation of the water, SEM visualization was performed. Results are shown in the matrix of images of figure 3.1. The first line of the image matrix corresponds to three bilayers, the second line to six bilayers and the last line to nine bilayers. Column one, two and three gather dipping times of 5, 10 and 15 minutes, respectively. The major changes results from a variation of the number of bilayers rather than the dipping time. Indeed, 3-bilayer nanotubes seem to flatten (they look like nanoribbons) and they are also twisted around their axis.

Flattening can be observed with SEM because it results in larger diameter. In figure 3.1, three flattened sections are shown (dotted green arrows). It was calculated that the average diameter of the 3-bilayer tubes amounts to at least 485 nm while it should be about 300 nm (like the pore diameter of the template). Lateral load is applied on the nanotubes upon tube collection and drying, due to an increase in van der Waals and capillary forces. For hollow cylinders, the lateral load has to be higher than $E(w/D_0)^3$ for the tube to flatten. E is the Young's modulus, w the wall thickness and D_0 the external tube

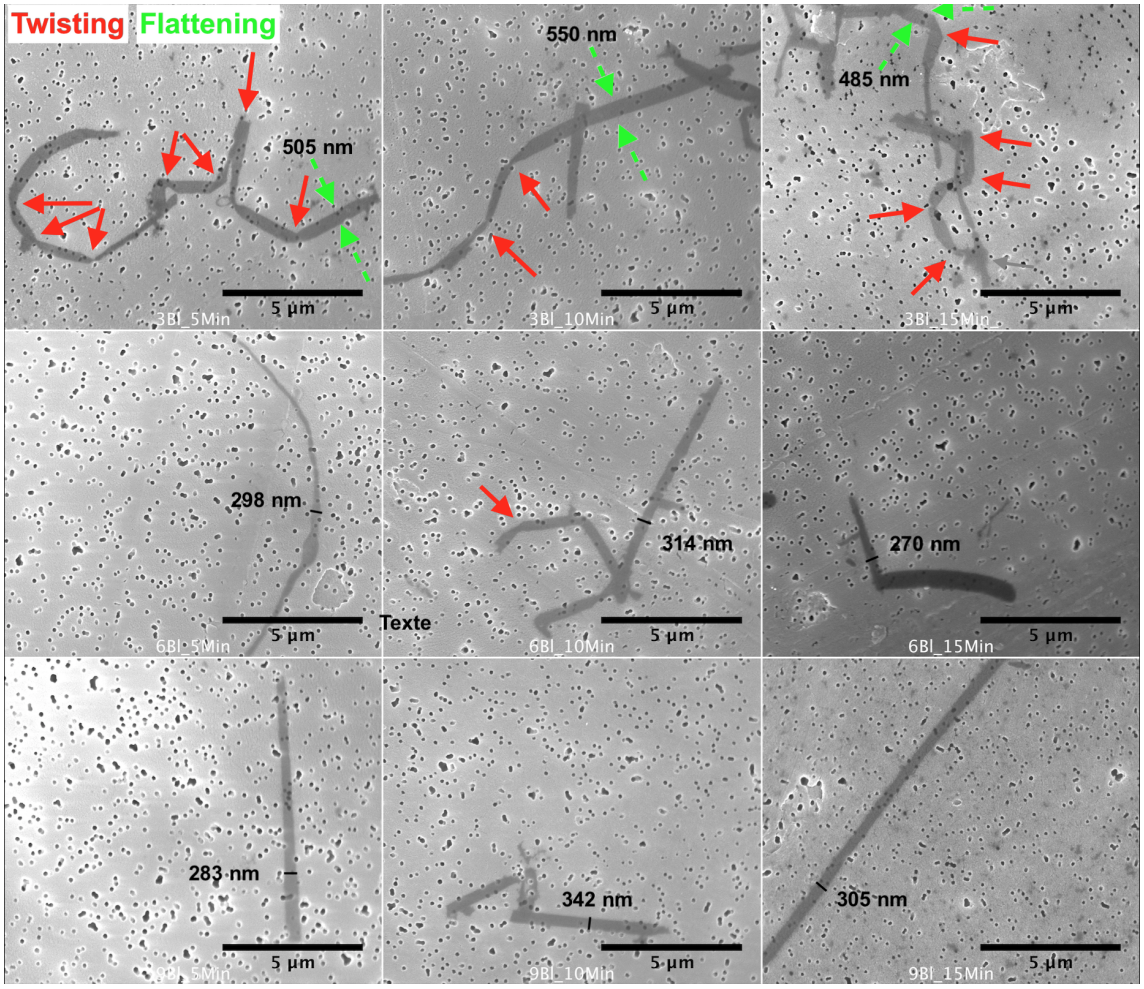

Figure 3.1: Matrix of SEM images of PSS/PAH nanotubes. Lines represent the number of bilayers (3-6-9) from top to bottom and columns the dipping time (5-10-15 minutes) from left to right.

radius. [2] The Young's modulus is $\propto R_{EE}^2/L$ with R_{EE} the root-mean-square *end-to-end* distance of the tube and L the contour length [54]. It is easy to see that R_{EE} is smaller for nanotubes built with fewer bilayers and that the more bilayers, the higher R_{EE}. One can assume that L is the same for all the tubes (i.e., they were not broken in the process) as well as D_0, and that they are fixed by the thickness and the pore diameter of the PC membrane template (25 µm and 300 nm, respectively). The Young's modulus therefore is smaller for the 3-bilayer nanotubes and increases with the amount of layers. Moreover, w (the wall thickness) should also be smaller for three bilayers than six or nine. It leads to the conclusion that the fewer bilayers there are, the smaller is the minimum lateral load needed for a flattening. This is why flattening is observed for tubes with three bilayers and not for the others.

Nanotubes built with only three bilayers undergo twisting (full red arrows). Nanotube resistance to twisting is also proportional to E, which explains the huge amount of twisted sections for 3-bilayer nanotubes, while there is almost none for the other tubes.

At this stage of the characterization of the 3-6-9 bilayers tubes built with 5-10-15 min-

utes in the solutions, dipping time does not seem to have an impact on the nanotube morphology.

3.1.2 Nanotube wall thickness

Porometry measurements allowed to determine the nanotube wall thickness. Results are shown in figure 3.2. These results show that the dipping time influences the tubes morphology, on contrary to what was observed with the SEM images. Indeed, in the graph, it can be seen that the thickness of the nanotube wall increases with the dipping time. As explained in section 1.3.7, the adsorption on a pore wall begins rapidly without diffusion limitation. Then, adsorbed chains interconnect through the pore and a dense gel is formed. The diffusion limits the deposition of further layers and the process becomes slower. One could think that the dipping time dependence of the nanotube wall thickness is due to a pore filling reached before the deposition of the third bilayer. Indeed, if the pore was not filled, the assembly of the layers would not depend on the dipping time, as the diffusion is not a limiting mechanism before the formation of the dense gel. However, if the pore was filled, the thickness of the layers would not change as much as it is shown in the graph, which rejects the pore filling hypothesis. The dipping time dependence of the nanotube wall thickness is probably due to the sensitivity of the porometry measurements to local restrictions of the section. It is possible that, in the nanotube, there is a constriction at a given point (the ends being more likely), and that this constriction increases over time. The gas flow will therefore be significantly impacted, giving a time dependency of the nanotube wall thickness, while their overall appearance is not influenced.

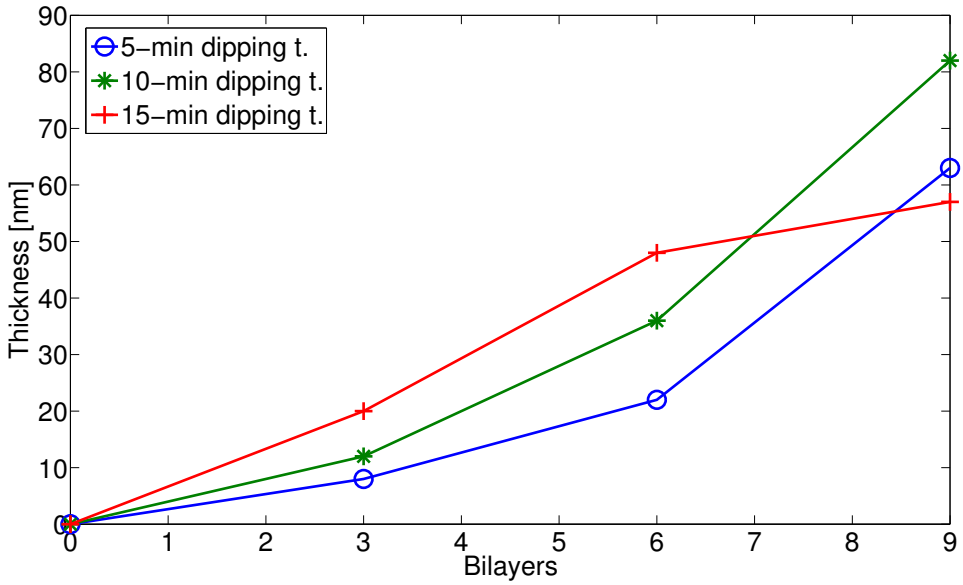

Figure 3.2: Nanotube wall thickness depending on the amount of bilayers and the dipping time.

15-min dipping time curve shows a very small increase between six and nine bilayers, in comparison to the other curves. A hypothesis could be that decrusting step was badly performed after six bilayer deposition. Pores were therefore clogged and polyelectrolytes could not adsorb on their walls.

The growth seems exponential. It is not unexpected because the linear growth regime of PAH-PSS multilayer is known for assembly on flat surfaces, and not for membrane templated assembly. The mechanism of growth inside nanopores is different from the one on flat surfaces. However, more samples should be done (for example, measuring the porometry after each bilayer) in order to conclude that with a pH between 6.5 and 7, the nanotube wall thickness growth is exponential. This is beyond the scope of this work.

3.1.3 Mats

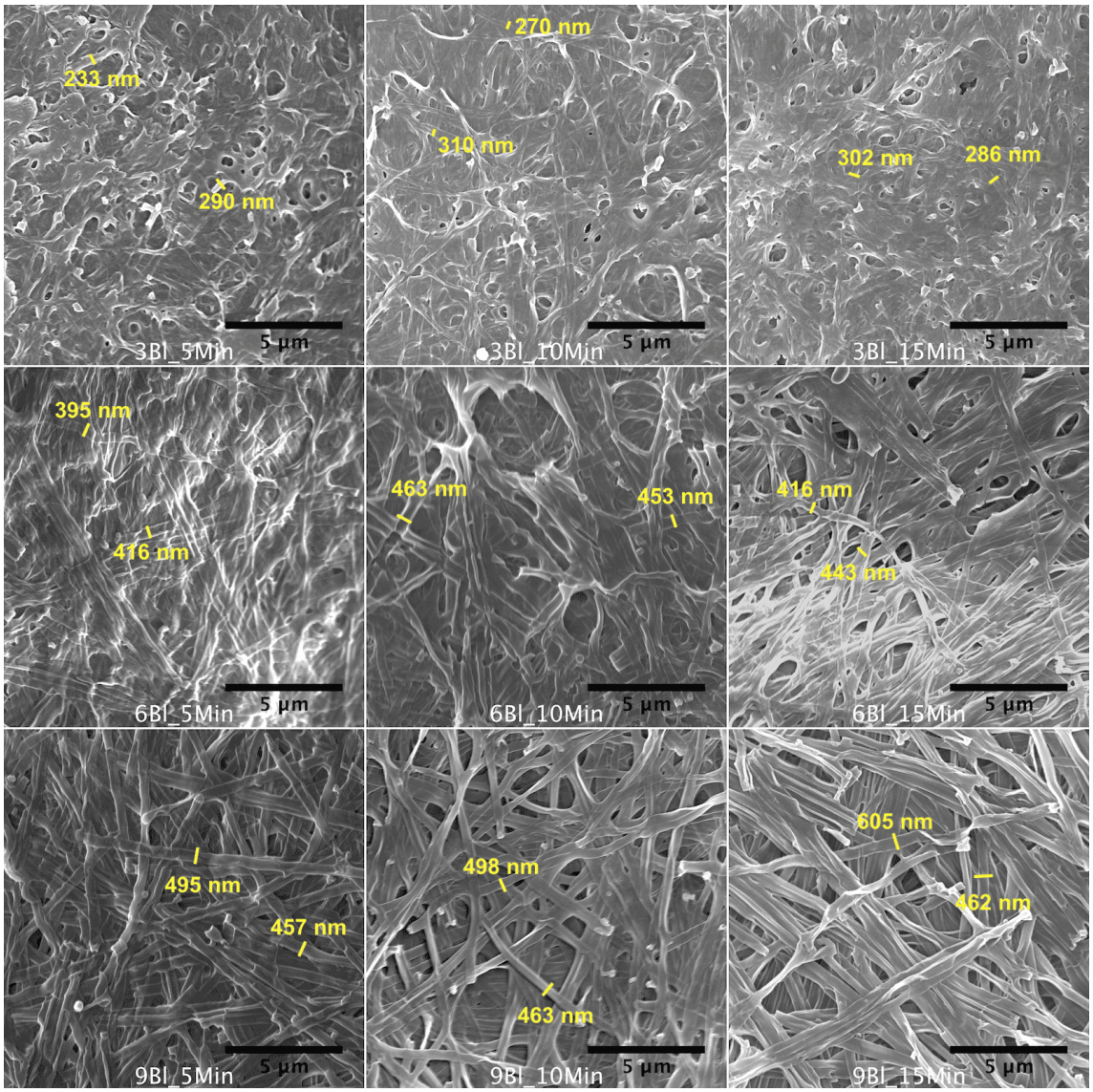

Figure 3.3: Matrix of SEM images of PSS/PAH nanotubes mats. Lines represent the number of bilayers (3-6-9) from top to bottom and columns the dipping time (5-10-15 minutes) from left to right.

The suspension of the tubes in water was filtered on a PET membrane to build a mat. A gold coating was then performed to observe the papers by SEM. Figure 3.3 shows images of the samples. The same matricial organization as for the tubes in suspension was kept

for the images: the amount of bilayers increases from line to line, and dipping time from column to column.

Again, the amount of bilayers impacts the morphology of the mats more than the dipping time. Mats of coarser texture were obtained with nanotubes of fewer bilayers. Indeed, tubes merge with each other because of electrostatic interactions. With the increase of number of bilayers, the tubes are stiffer (higher Young's modulus). They therefore provide more resistance to this merging and the mats morphology is better defined. [2]

In section 3.1.1, it was concluded that only the 3-bilayer nanotubes flattened, and that it was because of drying. However, in figure 3.3, it can be seen that $(PAH/PSS)_6$ and $(PAH/PSS)_9$ nanotubes also flatten. Their diameter is larger than the one of the PC membrane template. Measured diameter of the 3-bilayer nanotubes in mats is kept around 300 nm (or even smaller). However, as the tubes merged a lot, these results are not statistically significant. For mats, the origin of the flattening is not the drying (since 6- and 9-bilayers nanotubes did not flatten upon drying!), but it is probably due to the compressive forces induced by the filtration step in the paper built-up process.

Porosity of the papers is also observable, and seems to increase with the rigidity of the nanotubes.

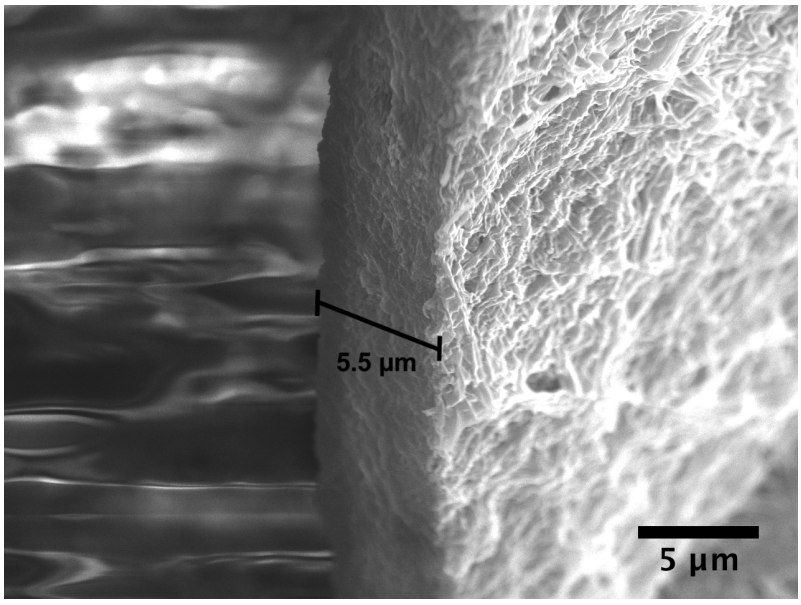

Figure 3.4: SEM image of $(PAH/PSS)_6$ nanopaper placed vertically. Dipping time was 10 minutes. The mat contained $2.5 \cdot 10^9$ nanotubes (5x5 cm^2 of PC membrane).

Figure 3.4 shows a SEM image of a paper placed vertically. The nanotubes had six bilayers and the dipping time was ten minutes. The thickness value of the sample was 5.5 µm. However, this value must be used carefully. Indeed, this sample was dried for SEM analysis, while in the further sections of the work, mats were kept in saline solution. Therefore, the tubes are swelled and the thickness could be larger. This image also gives an idea of the paper surface morphology. Like in the work of Zhang *et al.*, clusters with larger density of tubes are noticeable. It confirms their hypothesis of a continuous mat formed by accumulation of tubes in local clusters, with progressively infilling of the

structure.

3.1.4 Conclusion

After the analysis of these results, it was decided to keep nine bilayers for the tubes, as the number of bilayers has a significant effect on the nanotube and mat morphology. 9-bilayers nanotubes showed a higher rigidity, and were less subject to deformations (flattening and twisting). In mats, these tubes led to a higher porosity and less fusion although they underwent flattening because of the compressive forces in the mat built-up. Dipping time was fixed at 10 minutes. It indeed allowed to reduce the nanotubes assembly time by 1h30, and the thickness of the tubes was high enough to build good mats. Therefore, for the rest of this work $(PAH/PSS)_9$ nanotubes were used, with a ten minutes dipping time.

3.2 Incorporation of particles in mats

After the optimization of the tube fabrication process, the next step of this work was to build a 3-layered paper. First and last layers were mats obtained after the filtration of ca. $2.5 \cdot 10^9$ suspended nanotubes in water. In the tube suspension of the middle layer were added $400 \cdot 10^6$ latex particles. Mechanical properties of this structure were studied and improved. Temperature effect was also analyzed. Finally, particle localization was determined.

3.2.1 Mechanical stability

After the 3-layered nanopaper built-up, the structure was kept in saline solution. Ultraviolet-visible spectroscopy of the supernatant was used to qualitatively check the decomposition of the paper. The graph shown in figure 3.5 represents the first results obtained on a 3-layered paper. This paper was placed in a saline solution directly after its built-up, for 2 hours. It was then transferred in a fresh solution for 2 more hours, and finally again in a fresh one over night.

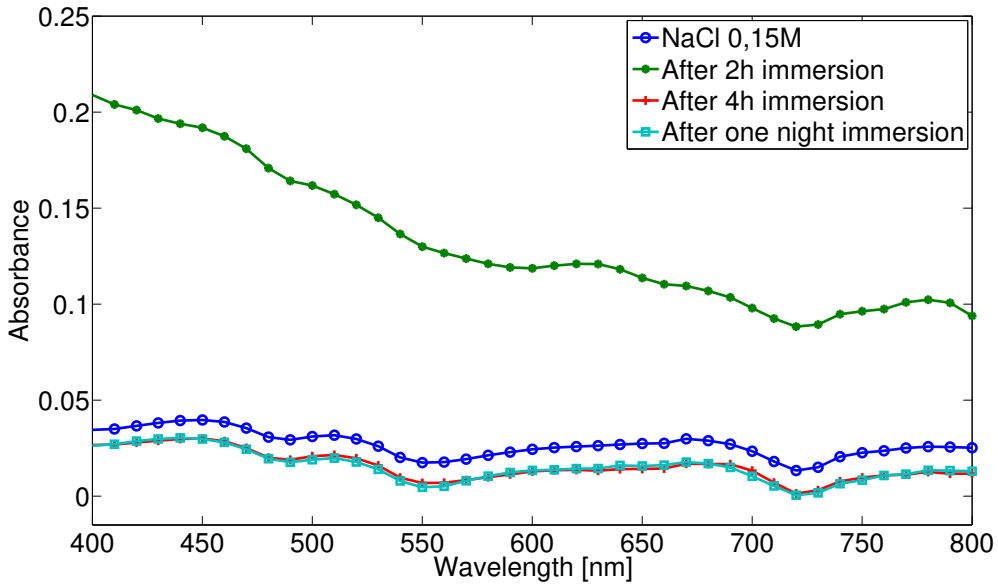

Figure 3.5: 3-layered paper supernatant ultraviolet-visible spectroscopy. Results after 2h, 4h and one night in saline solution. Blue open dots correspond to a control fresh saline solution without mat.

It is clear from the figure that the green line (full circles) has higher values than the others. This line corresponds to the first supernatant collected from the solution in which the paper was dipped. Other curves are similar to the control line (blue dotted one). Therefore, one can conclude that the structure partially decomposes directly after its build-up, and that after this decomposition, what remained of the structure was mechanically stable, as the red (crosses) and light blue (squares) curves show. However, the nature of the elements released in the saline solution was not known. It could be latex particles, that therefore were not trapped in the structure. It could also be loosely attached chunks of the complete structure, that were taken off because of the sample manipulation. To check the

nature of these released elements, the supernatant was observed by epifluorescence. Latex particles were tagged with a yellow-green fluorescent dye and observations indicated that PAH/PSS nanotubes were also slightly fluorescent in green. However, by selecting the range of wavelengths visualized by the epifluorescence microscopy, it is possible to select only the fluorescence of the particles or of the tubes, or a combination of these elements.

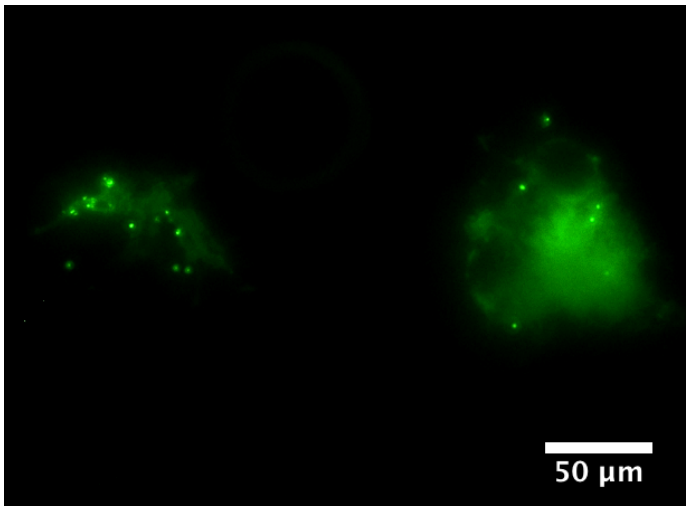

Figure 3.6: Epifluorescence microscopy of the supernatant of the solution in which the 3-layered paper was for 2 hours. Wavelength range kept for this image allows to visualize the particles and the nanotubes.

Figure 3.6 is an epifluorescence microscopy image of the supernatant of the solution in which the 3-layered paper was kept for 2 hours. Wavelength range for this image includes the particles and the nanotubes. It can be seen that the elements released in the saline solution were big chunks of paper, in which latex particles were entrapped. Indeed, two large (about 50 µm) zones of nanotube agglomeration are visible, as well as latex particles inside these zones. However, there are no particles outside the zones, and it confirms that particles are entrapped into the nanotubes network.

To improve the mechanical properties of the sample, we tried to play with two mechanisms:

1. The first one was the **adhesion** of the 3-layered nanopaper on its support. Indeed, big chunks collected in the supernatant could possibly come from poor adhesion of the nanopaper on the PET membrane used in the filtration process. Actually, when the samples were manipulated, it was already observable that elements of the system were not well fixed together, as figure 3.7 shows. To improve the adhesion, the PET membrane used in the filtration process was coated with polyethylenimine (PEI) alone and with PSS over the PEI. PEI was used as a coating because it is widely used as an attachment promoter. Moreover, assuming that the first PSS layer of the nanotubes was not complete, adding PSS on top of PEI should further promote the adhesion of the nanotubes on the coated membrane. Indeed, PSS was theoretically first adsorbed on the PC pore walls, but as the PC is slightly negatively charged, it is possible that the adherence of the PSS was not good. Therefore, the external surface of the tubes could be essentially made of positively charged PAH, and its contact with the PSS coating should improve the adhesion.

2. The second mechanism of improvement was the **cohesion** of the nanopaper. Two methods were tried. First, a LbL coating of $(PAH/PSS)_6$ was done over/in the whole structure (PET membrane-nanopaper). The LbL was supposed to maintain the structure entrapped. The other method tested was the formation of a PAH/PSS complex over/in the sample. A drop of PAH solution was first put in contact with the system (see figure 3.7). Its excess was carefully removed, before adding a drop of PSS solution. As they are oppositely charged polyelectrolytes, when their solutions are mixed together, a bulk complex is formed within the paper. This complex aimed at reinforcing the nanotube network.

Figure 3.7: Picture of a 3-layered nanopaper before adhesion improvement. A drop of polyelectrolyte was placed over the nanopaper, to form a complex to improve the cohesion of the structure.

Samples that were done are summarized in table 3.1. To see the influence of the latex particles on the mechanical properties of the nanopaper, four more samples were done without them. The 3-layered mat fabrication process was exactly the same, except that no particles were added in the middle layer tube suspension.

		Cohesion technique	
		Complex	LbL
Adhesion technique	PEI+PSS	1	1
	PEI alone	1	1

Table 3.1: Summary of samples tested for adhesion of the nanopaper on the PET membrane support, and improvement of the nanopaper cohesion.

UV-visible spectroscopy was performed on the samples. Results for the samples with latex particles are shown in figure 3.8, while the ones without them are in figure 3.9.

The effect of the latex particles is clearly visible. Curves of paper without particles are higher than the ones with them. It means that they increase the cohesion of the paper. As the particles are negatively charged (carboxylate groups), their positive effect on the cohesion confirms the previous assumption of a positively charged tube external surface. Indeed, if the nanotubes are mostly positively charged, electrostatic interactions between the two elements promote a better cohesion of the nanopaper.

It can be seen in figure 3.8 that the improved samples degraded less than the control paper. Combination of only PEI for the adhesion and PAH/PSS complex for the cohesion seemed to be less efficient than the other combinations. However, differences between the

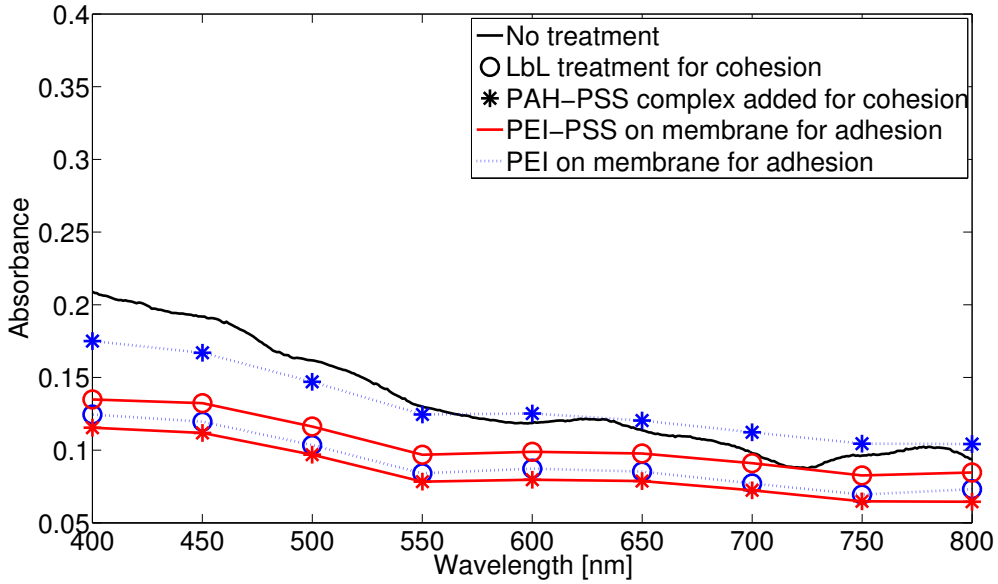

Figure 3.8: Ultraviolet-visible spectroscopy of paper supernatant (samples with particles).

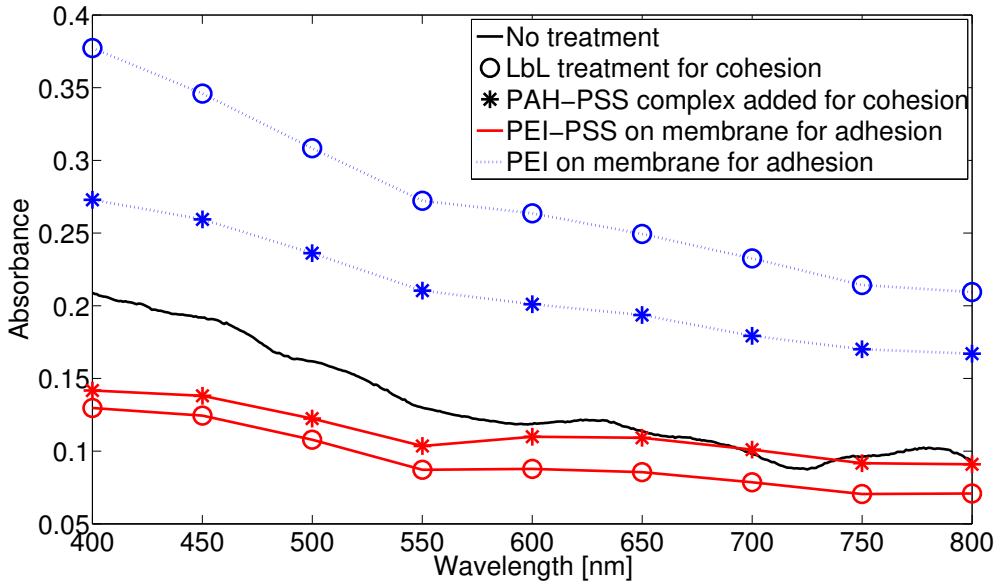

Figure 3.9: Ultraviolet-visible spectroscopy of paper supernatant (samples without particles, except for the black curve).

curves are weak, and an analysis of the supernatant by epifluorescence microscopy was thus done to determine the best combination. Results are shown in figure 3.10 in a matrix of images. Only the wavelength allowing to see the particles was used for these images.

For the adhesion technique, the first line of the matrix of images gathers the results of using a PEI+PSS coating and the second of using only PEI as coating. In the images of the samples with only PEI, collections of latex particles are visible. These collections confirm the previous hypothesis of big chunks pulled off the sample: if the particles are

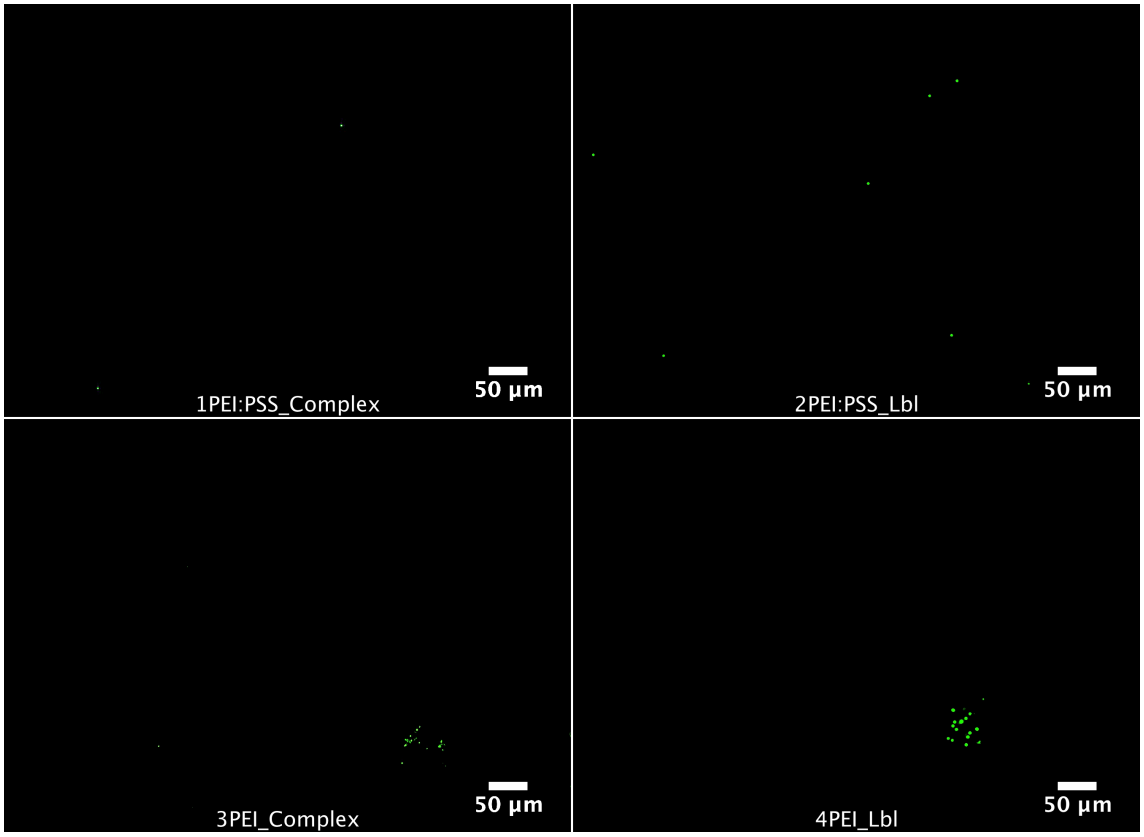

Figure 3.10: Epifluorescence microscopy of supernatant of a solution in which the improved nanopapers was immersed for 2 hours. The first line gathers papers with a PEI+PSS coating on the PET membrane, while only PEI was added over the PET in the samples of the second line. A PAH/PSS complex was formed in the structure for the samples of the first column and a $(PAH/PSS)_6$ LbL film was deposited on/in the nanopapers of the second column. The wavelength range kept for this image allows to see only the particles.

assembled in the image, it is because they are entrapped in the nanotube network, as shown in figure 3.6. These chunks are not visible for the samples with a PET membrane covered by a PEI+PSS coating. One can therefore conclude that the addition of PSS over the PEI improves the adhesion of the nanopapers on the PET, and it confirms once more that the external surface of the tubes is mostly positively charged.

The difference between the two tested cohesion methods is weaker than the one for the adhesion techniques. A few less free latex particles and chunks were found in samples with the PAH/PSS complex (column 1 of figure 3.10) than after the LbL deposition, but it was not enough to determine that one technique is better than the other. However, as the complexation is faster than the LbL technique, it was decided to keep this method.

To conclude this section on the mechanical stability, it was decided to coat the PET membrane of the next samples with a layer of (PEI/PSS) to improve the adhesion between the nanopaper and the membrane. It was also decided to form a PAH-PSS complex in the whole paper to maintain everything together.

3.2.2 Temperature effect

As the final goal of the 3-layered nanopaper is to use it as a patch containing bacteria on the skin, it was important to test its stability at 37°C, and its stability under movements. To do so, a sample was placed in a thermal agitator. The rotation speed was fixed at 500 rotation per minute. The sample was first kept in saline solution at ambient temperature without agitation for two hours. Then, it was transferred to a fresh solution and inserted in the agitator at 37°C. The operation was repeated after 30 minutes. Results are shown in figure 3.11. The curve named "0 min" is the spectra of the solution in which the paper was first kept without temperature and agitation. The curves "30 min" and "24 hours" represent the solution after 30 minutes and one day of thermal agitation. There is slightly more decomposition with temperature and agitation over the time, but the values are really small compared to the first samples (figure 3.5). On the basis of these results, it can be concluded that the paper is essentially thermally stable.

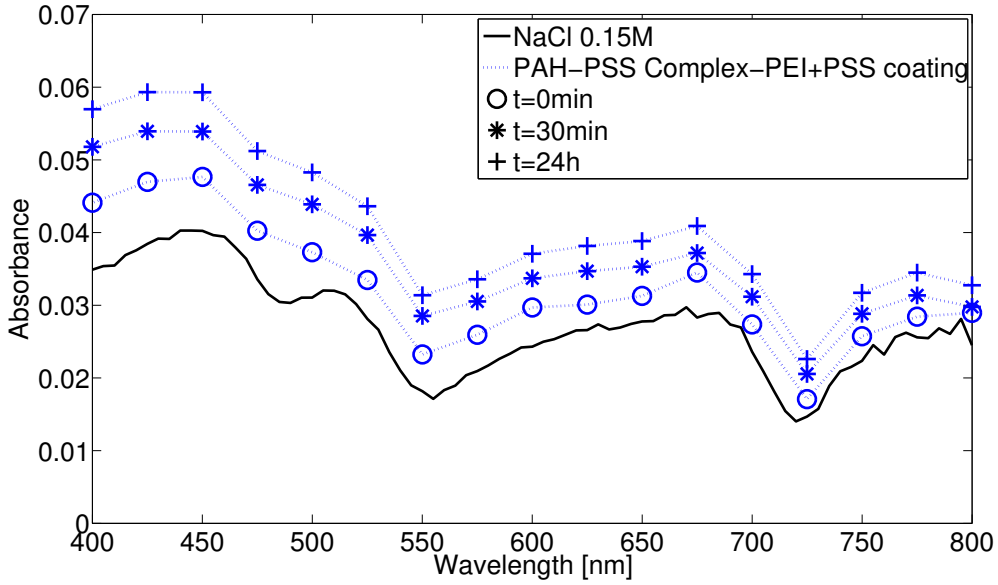

Figure 3.11: Ultraviolet-visible spectroscopy of the supernatent of a solution in which a sample was immersed and kept at 37°C for 0 min, 30 min and 24 hours. Black curve reflects the UV-visible spectroscopy of a control solution of NaCl 0.15M.

3.2.3 Particles localization

The final step of the 3-layered nanopaper analysis of this work was to determine the localization of the latex particles in the paper. For the application, it was desirable that the particles stayed in the middle layer, but it was possible that through the fabrication process, they migrated. Microtomy was used to obtain 1 µm slices perpendicular to the plane of the paper. Then, the cuts were observed by optical microscopy. An example is presented in figure 3.12. With this observation, it was possible to manually count the amount of particles on a surface, and therefore, to determine their density. Results are summarized in table 3.2 for two samples. These samples were improved by the two methods selected before (section 3.2.1).

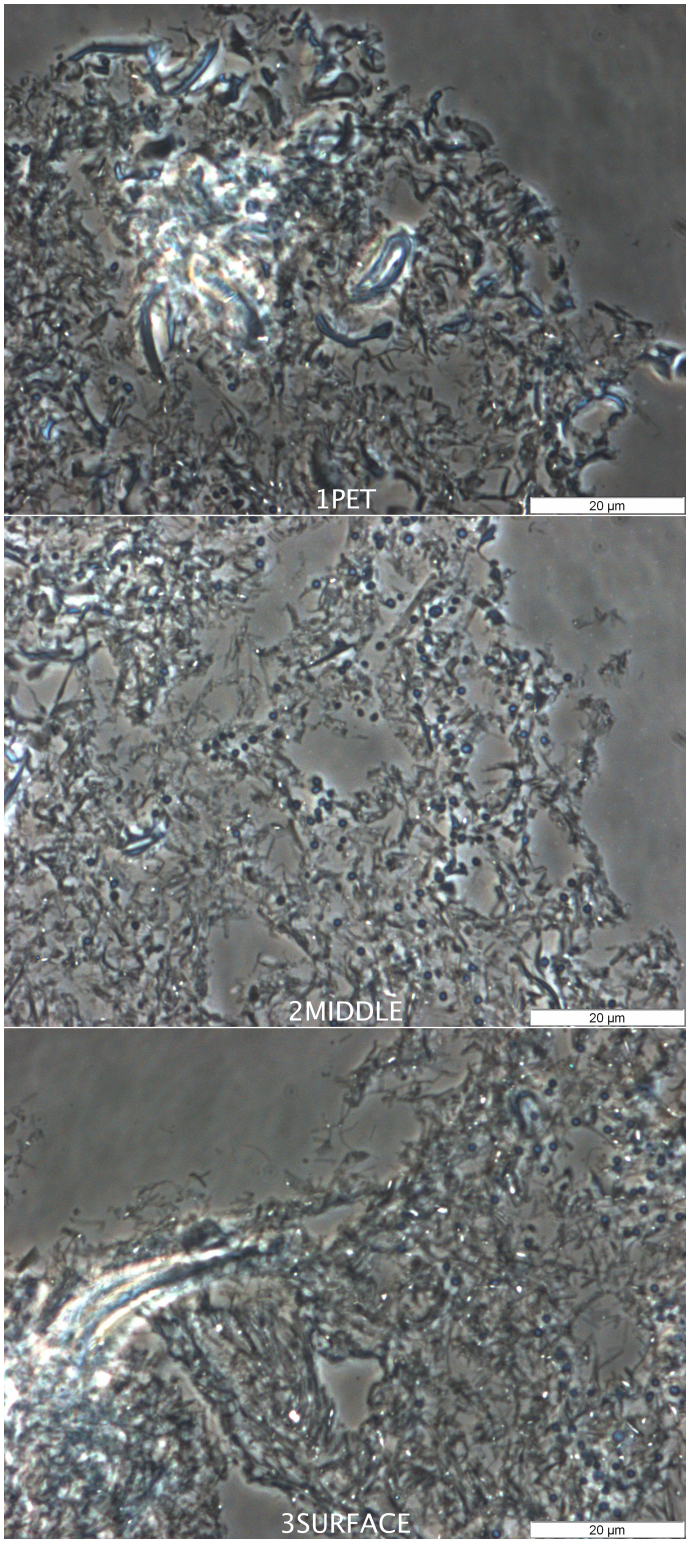

Figure 3.12: 1 µm slice of 3-layered nanopaper containing nanoparticles observed by optical microscopy. Localizations in the paper are: close to the PET membrane (top image), middle of the nanopaper (middle image and right of bottom image) and close to free surface (left of bottom image).

	Localization	Area [μm^2]	Latex particles	Density [$/\mu m^3$]
Sample 1	Surface	2651	3	$1.13 \cdot 10^{-3}$
	Middle	5267	126	$23.92 \cdot 10^{-3}$
	PET	4564	32	$7.01 \cdot 10^{-3}$
Sample 2	Surface	3771	4	$1.06 \cdot 10^{-3}$
	Middle	5779	146	$25.26 \cdot 10^{-3}$
	PET	4200	1	$0.24 \cdot 10^{-3}$

Table 3.2: Summary of the latex particle count for two samples.

The technique used to determine the particles density is not very accurate, but was useful to confirm that most of the particles were in the middle layer. Indeed, it was possible to compare the results of the table 3.2 to what was already known: $400 \cdot 10^6$ particles were added to the nanotubes collected from 5x5 cm^2 of PC membrane. The diameter of the mat was determined by the filtration set-up, and its approximate thickness was already obtained thanks to figure 3.4. Therefore, the theoretical density was 0.47 particles/μm^3. It differs by an order of magnitude compared to the results of counting. This difference can be easily explained by the assumption on the thickness of the mat (figure 3.4) and statistical errors on counting. It can also be due to a very slight migration of some particles in the other layers (as in the table), and a loss of them in the 3-layered nanopaper built-up. Despite this difference between the theoretical value and the results, it can still be concluded that the particles stayed mostly in the middle layer, as wanted.

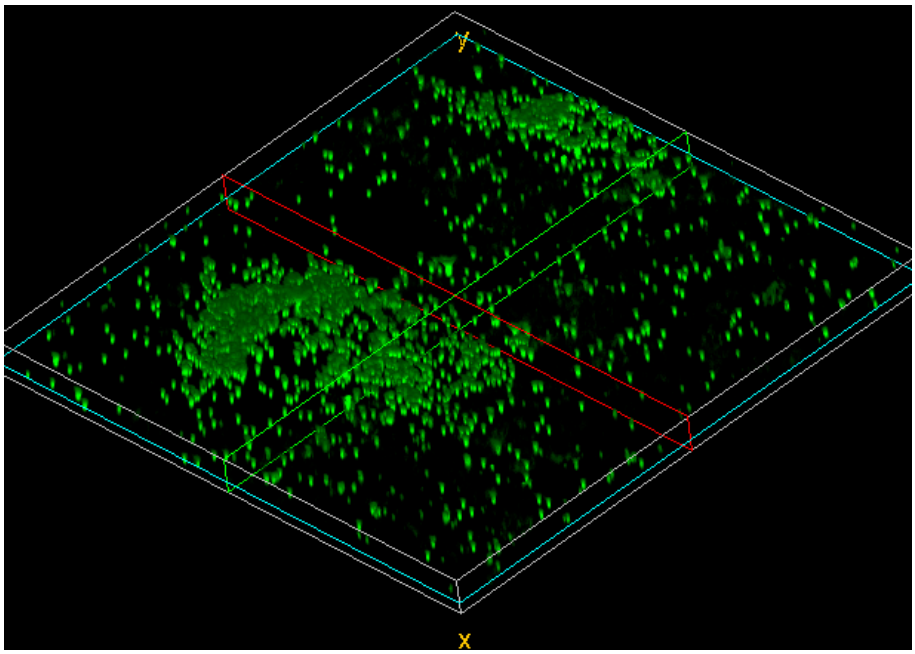

Figure 3.13: 3D-View by confocal microscopy of a 3-layered nanopaper. Wavelength range kept for this image is selected to see only the particles.

Confocal microscopy confirmed also the localization of the particles: a 3D-view is presented in figure 3.13, as well as a mean grey value along the thickness of a 3-layered nanopaper (figure 3.14). The mean grey value of the images is related to the distribution of the particles. Indeed, the light seen on the images is due to the fluorescence of the

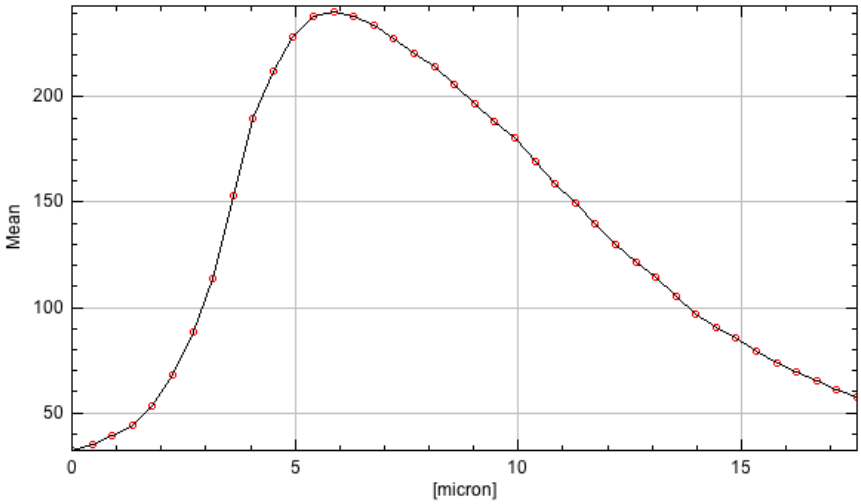

Figure 3.14: Mean grey value along the thickness of a 3-layered nanopaper imaged by confocal microscopy. For the x-axis, the origin corresponds to the surface of the nanopaper, and the x value is increased while going deeper in the paper.

particles. They are mostly in the middle of the nanopaper. A steep increase is obtained between the top layer of nanopaper and the middle layer, while the decrease between the middle and the bottom layer is softer. Particles are more subject to migration towards the PET membrane because of the compressive forces of the filtration process used to built the nanopaper. The results on the graph confirm also that the thickness of the layers is approximatively 5.5 µm.

One can also see in the 3D-view that the particles are also assembled in clusters. By adding the wavelength range of the nanotubes for the image (figure 3.15), it was seen that there are more particles where there are more tubes (remember the nanopaper formation by the accumulation of the tubes in clusters followed by the structure in-filling). It was even observed that the particles situated outside of these clusters were able to move. They were moving back and forth. On the contrary, in the zones with a larger density of tubes, the particles did not move at all. This observation confirms once more that the nanotube network is efficient at encapsulating the latex particles.

3.2.4 Conclusion

After this part of the work, a mechanically and thermally stable structure was obtained. Indeed, the mechanical stability of the 3-layered nanopaper was improved by a (PEI/PSS) coating of the top of the PET membrane used as support, and by the addition of a PAH-PSS complex in the nanotube network. This improved structure showed good stability under movements at 37°C, and the particles were localized as wanted in the middle layer. At that point, it could be concluded that the structure is suitable for the application. However, the polymers used are not yet suitable for the envisioned application since they are not skin-compatible.

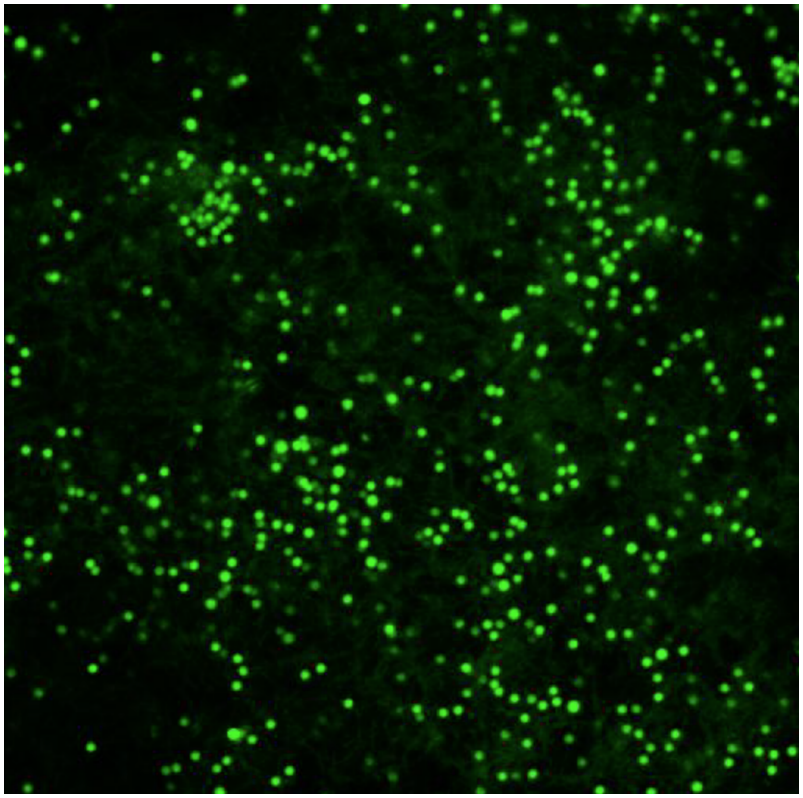

Figure 3.15: Confocal image of the middle layer of a 3-layered nanopaper. Wavelength range kept for this image allows to see the particles and the nanotubes.

3.3 Transposition to biobased polymers

The last part of this work concerns a preliminary research for a transposition to biobased polymers. Indeed, as the patch is designed to be in contact with the skin, it should be biocompatible. PAH and PSS were therefore replaced by glycol chitosan (gCHT) and alginate (ALG). The complexation in the structure was tested with these new polymers. LbL on flat surface was also investigated, and finally mats of gCHT/ALG nanotubes were even built.

3.3.1 Complex formation in nanopaper

Results of stability under movements of two nanopapers covered with a PAH/PSS and a ALG/gCHT complex at 37°C are shown in figure 3.16. The same procedure as the one described in section 3.2.2 was followed. The biobased polymer complex seems to be even better than the one with the previous polymers, but the difference is very slight. These polymers represent a good skin-compatible solution.

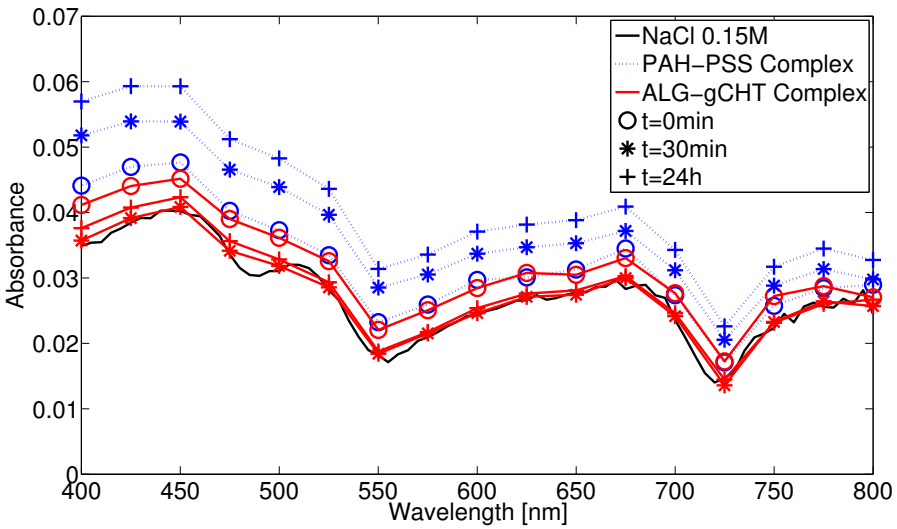

Figure 3.16: Ultraviolet-visible spectroscopy of the supernatant of a solution in which samples were immersed and kept at 37°C for 0 min, 30 min and 24 hours. The first sample is covered with a PAH/PSS complex (dotted blue curve) and the second sample by a ALG/gCHT one (red curve). The black curve is the UV-visible spectroscopy of a control solution of NaCl 0.15M.

3.3.2 Layer-by-Layer on flat surface

To characterize the growth regime of gCHT/ALG LbL films at pH 7, the thickness of the deposited film on the surface was measured after each layer by ellipsometry. Results are shown in figure 3.17. The growth regime is exponential. It was expected since gCHT and ALG are weak polyelectrolytes (see section 1.3.3). From 5 bilayers, the error bar increased a lot, probably due to the roughness of the samples. AFM characterization was performed to check this hypothesis. Results are in figure 3.18. The first 3D-projection is for two assembled bilayers, the second for four bilayers and the third for six. The results are consistent with the ones obtained by Saghazadeh *et al.*: small island-shaped patches are

formed on the surface at the beginning of the multilayer assembly, and these islands widen with the number of layers [23]. Therefore the roughness is increased by the assembly of the layers, leading to large dispersion for the thickness.

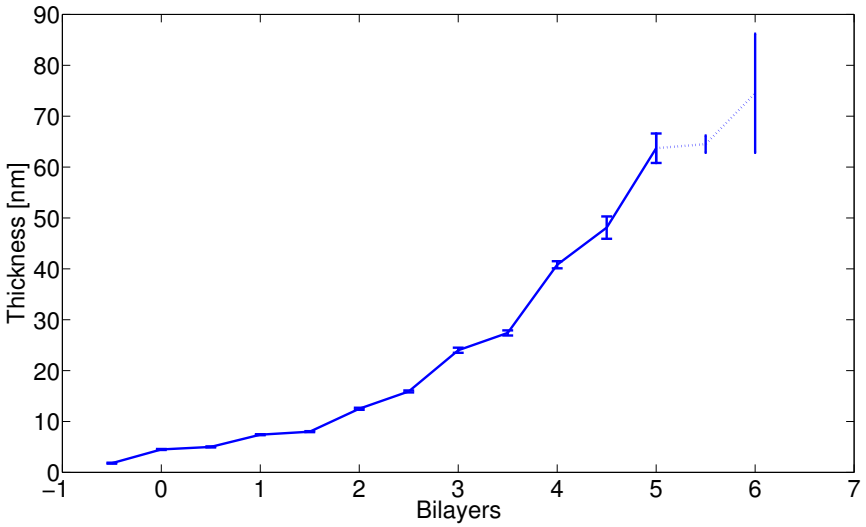

Figure 3.17: Thickness of gCHT/ALG LbL films after each polyelectrolyte deposition, obtained by ellipsometry.

3.3.3 Nanopapers of Layer-by-Layer nanotubes

Mats of nanotubes with three, six and nine bilayers were assembled with ten minutes dipping time. Then they were observed by SEM. They are shown in figure 3.19. The first, second and third images are mats made of 3-, 6- and 9-bilayers nanotubes, respectively. Nanotubes are visible in the mat formed from nanotubes with three bilayers, but not in the other mats. It seems that they are sticked together. A hypothesis is a bad dissolution of the polycarbonate membrane, that could be due to a greater adhesion of the polymers on it. Another explanation for the fusion of the tube is directly linked to the tubes: the Young's modulus of gCHT/ALG nanotubes is smaller, and the tubes are more swollen than the ones made of PSS/PAH. Therefore, the structure is softer and, under drying, nanotubes are flattened, leading to this appearance of tube fusion. To confirm this hypothesis, one can mark the tubes and observe them with epifluorescence. Nanotubes suspended in water should also be observed to characterize better their behaviour, and particularly to determine how many bilayers should be assembled.

3.3.4 Conclusion

In this section, the first steps of a transposition to biobased polymers were investigated. The PAH/PSS complexation over the sample to increase its stability can be clearly replaced by a ALG/gCHT one, with the same results. The growth regime of gCHT/ALG film on flat surface is exponential, and roughness increases with the assembly. Finally, mats showed a fusion of the tubes. However, this fusion cannot be completely understood without further characterization. The gCHT/ALG combination seems to be promising to replace the PSS/PAH one, but more investigations should be performed.

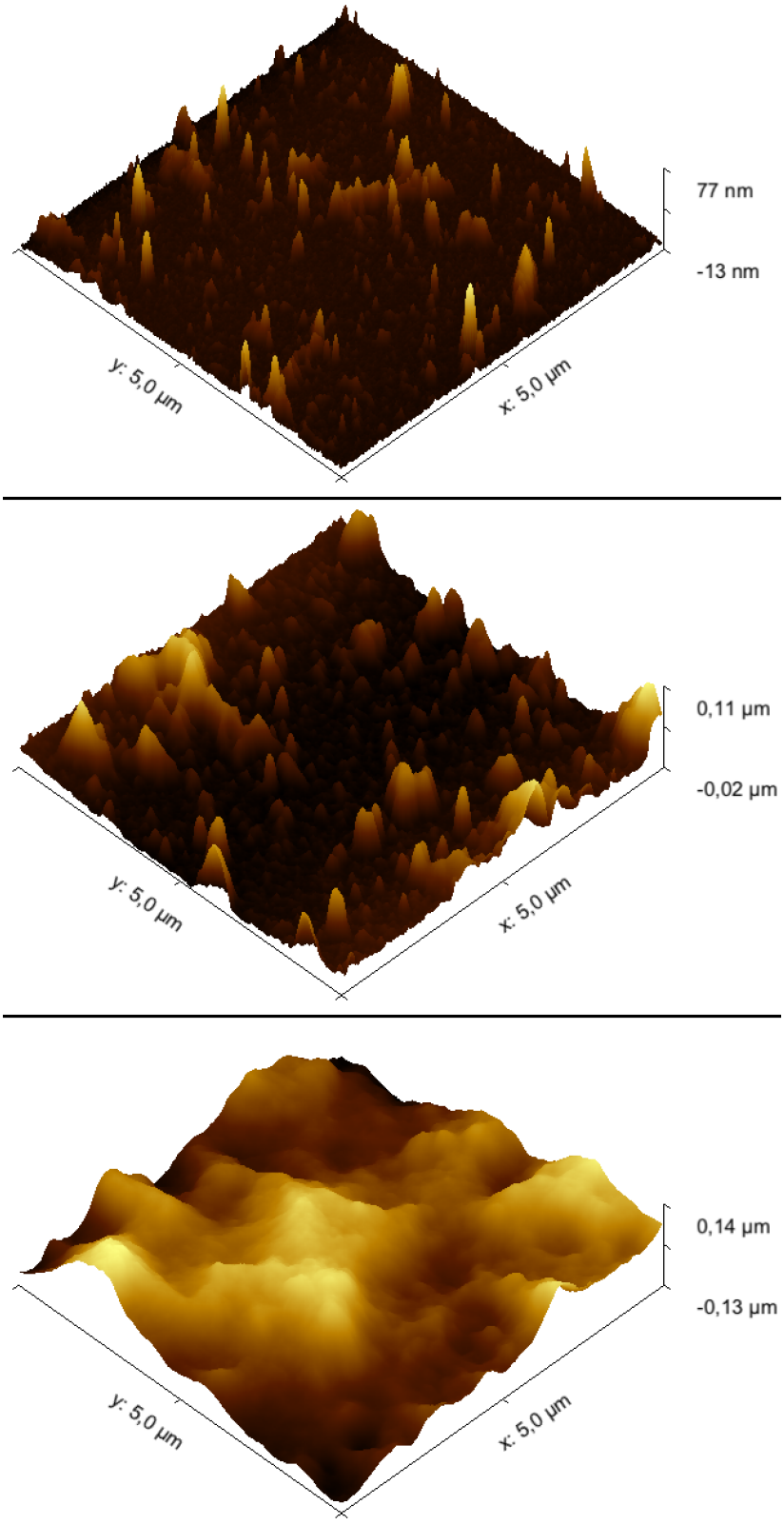

Figure 3.18: AFM 3D-projection of gCHT/ALG LbL on flat surface. Two, four and six multilayers were deposited for the first, the second and the third projection, respectively.

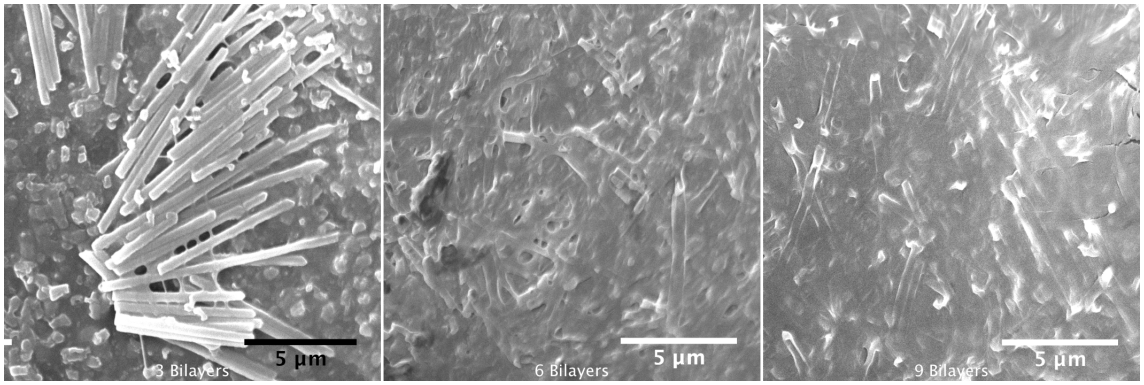

Figure 3.19: SEM images of gCHT/ALG nanotube mats, with increasing number of bilayers (3-6-9). Dipping time of 10 minutes.

Conclusions and perspectives

The aim of this work was to develop and characterize a sturdy 3-layered nanopaper containing particles, modeling bacteria. Indeed, the presence of some bacteria on the skin microbiome is essential, because the bacteria produces agents required for adherence, remodeling, nutrients release, protection against other bacteria and inhibition of uncontrolled inflammation [3]. In case of lack or absence of the bacteria on the skin, the host is vulnerable to colonization of the skin by pathogens and is less able to fight back the inflammation and keep the skin healthy. The medical patches designed in this work could bring the bacteria back on the skin of the host to ensure their positive functions.

First, the best amount of layers for the tubes and the membrane dipping time in the tube built-up were determined. Tubes suspended in water were observed by SEM. It was shown that tubes made of three bilayers undergo twisting and flattening much more than nanotubes with six and nine bilayers. The stiffness of the nanotubes also increased with the number of bilayers. Then, suspended nanotubes were collected in mats and observed. Mats formed from nanotubes with three bilayers presented a fusion of the tubes, while an increase in bilayer number led to less fusion. Flattening occured for all the tubes in the mats, because of the compressive forces in the mat built-up. For the two types of sample, no effect of dipping time was clearly observable, but porometry measurements were performed to determine the thickness of the nanotube walls. It increased with the dipping time. At the end of the section, it was decided to keep nine bilayers for the tubes while decreasing the dipping time to ten minutes, allowing to save 1h30 in the fabrication process.

The second part of the research concerned the 3-layered mats with the particles in the middle layer. First, the mechanical stability was qualitatively analyzed thanks to UV-spectroscopy of the supernatant of the samples after immersion in solutions, in which the sample partially decomposed. It was observed that the decomposition occurs only at the beginning, when the nanopaper is first dipped in the solution. Big chunks of the sample detached, but the particles remained entrapped in the paper. To avoid this decomposition, the adhesion of the paper on its support and the cohesion of the whole structure were improved thanks to an additional coating over the support, and a complexation over/in the nanotube network. The mechanical stability at 37°C and under movement was tested, as the paper has to be kept on the skin. With the adhesion and cohesion improvements, the paper proved to be stable under these conditions. Finally, the localization of the particles was determined. As wanted, the biggest part of them is localized in the middle of the nanopaper. There are more particles where there are more nanotubes, which shows that the entrapping of the particles is efficient.

The third and last part of this master thesis was about the research of a transposition to

biobased polymers. The complexation with biobased polymers showed to be as efficient as the one with synthetic polymers. Then, layer-by-layer on flat surface was performed to characterize the growth regime. It was determined thanks to ellipsometry that the growth is exponential, but from 5 bilayers the roughness of the sample was too high to have good measurements. Atomic-force microscopy confirmed this roughness. Finally, nanopapers of biobased nanotubes were done, and observed by SEM. A huge fusion between the tubes occurred, decreasing the porosity of the sample, due to the softness of these multilayers.

In conclusion, this work showed that the design is suitable for the application. Indeed, the particles were well entrapped in the network, and with the improvement of the adhesion and cohesion, the sample was mechanically stable. It is also possible to transfer the work to biobased polymers, even though further investigations need to be performed. For example, to reinforce the biobased nanotubes, one can imagine to begin the LbL deposition with biobased polymers and finalize the tubes with synthetic polymer adsorption, as Zhang *et al.* did [62]. It will provide a stiff core for the tubes. Another research that needs to be conducted, is a replacement of the PC membrane for the templating of the tubes. Indeed, to dissolve the polycarbonate, solvent is used, and this process is not skin-compatible. Finally, the next step of the work is to replace the latex particles by bacteria.

Bibliography

[1] B. Sun, Y. Long, H. Zhang, M. Li, J. Duvail, X. Jiang, and H. Yin, "Advances in three-dimensional nanofibrous macrostructures via electrospinning," *Progress in Polymer Science*, vol. 39, no. 5, pp. 862–890, 2014.

[2] S. Zhang, C. Vlémincq, D. R. Wong, D. Magnin, K. Glinel, S. Demoustier-Champagne, and A. M. Jonas, "Nanopapers of layer-by-layer nanotubes," *Journal of Materials Chemistry B*, vol. 4, no. 47, pp. 7651–7661, 2016.

[3] N. Fyhrquist, A. Salava, P. Auvinen, and A. Lauerma, "Skin biomes," *Current allergy and asthma reports*, vol. 16, no. 5, 2016.

[4] M. J. Blaser and S. Falkow, "What are the consequences of the disappearing human microbiota?," *Nature Reviews Microbiology*, vol. 7, no. 12, pp. 887–895, 2009.

[5] A. Cogen, V. Nizet, and R. Gallo, "Skin microbiota: a source of disease or defence?," *British Journal of Dermatology*, vol. 158, no. 3, pp. 442–455, 2008.

[6] M. Vemmer and A. V. Patel, "Review of encapsulation methods suitable for microbial biological control agents," *Biological Control*, vol. 67, no. 3, pp. 380–389, 2013.

[7] U. Prüße, J. Dalluhn, J. Breford, and K.-D. Vorlop, "Production of spherical beads by jetcutting," *Chemical Engineering & Technology: Industrial Chemistry-Plant Equipment-Process Engineering-Biotechnology*, vol. 23, no. 12, pp. 1105–1110, 2000.

[8] A. V. Patel and K.-D. Vorlop, "Entrapment of biological control agents applied to entomopathogenic nematodes," *Biotechnology techniques*, vol. 8, no. 8, pp. 569–574, 1994.

[9] A. Martinsen, G. Skjåk-Bræk, and O. Smidsrød, "Alginate as immobilization material: I. correlation between chemical and physical properties of alginate gel beads," *Biotechnology and bioengineering*, vol. 33, no. 1, pp. 79–89, 1989.

[10] K. Damodharan, S. A. Palaniyandi, S. H. Yang, and J. W. Suh, "Co-encapsulation of lactic acid bacteria and prebiotic with alginate-fenugreek gum-locust bean gum matrix: Viability of encapsulated bacteria under simulated gastrointestinal condition and during storage time," *Biotechnology and Bioprocess Engineering*, vol. 22, no. 3, pp. 265–271, 2017.

[11] M. Sittinger, B. Lukanoff, G. Burmester, and H. Dautzenberg, "Encapsulation of artificial tissues in polyelectrolyte complexes: preliminary studies," *Biomaterials*, vol. 17, no. 10, pp. 1049–1051, 1996.

[12] M.-C. Raymond, R. J. Neufeld, and D. Poncelet, "Encapsulation of brewers yeast in chitosan coated carrageenan microspheres by emulsification/thermal gelation," *Artificial cells, blood substitutes, and biotechnology*, vol. 32, no. 2, pp. 275–291, 2004.

[13] D. Poncelet, B. P. De Smet, C. Beaulieu, M. Huguet, A. Fournier, and R. Neufeld, "Production of alginate beads by emulsification/internal gelation. ii. physicochemistry," *Applied microbiology and biotechnology*, vol. 43, no. 4, pp. 644–650, 1995.

[14] A. J. Priya, S. Vijayalakshmi, and A. M. Raichur, "Enhanced survival of probiotic lactobacillus acidophilus by encapsulation with nanostructured polyelectrolyte layers through layer-by-layer approach," *Journal of agricultural and food chemistry*, vol. 59, no. 21, pp. 11838–11845, 2011.

[15] A. M. Jonas, K. Glinel, A. Behrens, A. C. Anselmo, R. Langer, and A. Jaklenec, "Controlling the growth of staphylococcus epidermidis by layer-by-layer encapsulation," *ACS applied materials & interfaces*, 2018.

[16] M. Gensheimer, A. Brandis-Heep, S. Agarwal, R. K. Thauer, and A. Greiner, "Polymer/bacteria composite nanofiber nonwovens by electrospinning of living bacteria protected by hydrogel microparticles," *Macromolecular bioscience*, vol. 11, no. 3, pp. 333–337, 2011.

[17] H.-W. Tong, B. R. Mutlu, L. P. Wackett, and A. Aksan, "Manufacturing of bioreactive nanofibers for bioremediation," *Biotechnology and bioengineering*, vol. 111, no. 8, pp. 1483–1493, 2014.

[18] S. Klein, R. Avrahami, E. Zussman, M. Beliavski, S. Tarre, and M. Green, "Encapsulation of pseudomonas sp. adp cells in electrospun microtubes for atrazine bioremediation," *Journal of industrial microbiology & biotechnology*, vol. 39, no. 11, pp. 1605–1613, 2012.

[19] S. Klein, J. Kuhn, R. Avrahami, S. Tarre, M. Beliavski, M. Green, and E. Zussman, "Encapsulation of bacterial cells in electrospun microtubes," *Biomacromolecules*, vol. 10, no. 7, pp. 1751–1756, 2009.

[20] F.-X. Xiao, M. Pagliaro, Y.-J. Xu, and B. Liu, "Layer-by-layer assembly of versatile nanoarchitectures with diverse dimensionality: a new perspective for rational construction of multilayer assemblies," *Chemical Society Reviews*, vol. 45, no. 11, pp. 3088–3121, 2016.

[21] J. Saqib and I. H. Aljundi, "Membrane fouling and modification using surface treatment and layer-by-layer assembly of polyelectrolytes: state-of-the-art review," *Journal of Water Process Engineering*, vol. 11, pp. 68–87, 2016.

[22] Y. Li, X. Wang, and J. Sun, "Layer-by-layer assembly for rapid fabrication of thick polymeric films," *Chemical Society Reviews*, vol. 41, no. 18, pp. 5998–6009, 2012.

[23] S. Saghazadeh, *"Polyelectrolyte multilayer nanotubes for drug delivery applications"*. PhD thesis, UCL-Université Catholique de Louvain, 2015.

[24] C. Peng, *Electrostatic layer-by-layer assembly of hybrid thin films using polyelectrolytes and inorganic nanoparticles*. Georgia Institute of Technology, 2011.

[25] J. B. Schlenoff and S. T. Dubas, "Mechanism of polyelectrolyte multilayer growth: charge overcompensation and distribution," *Macromolecules*, vol. 34, no. 3, pp. 592–598, 2001.

[26] X. Arys, A. Jonas, A. Laschewsky, R. Legras, and F. Mallwitz, "Layered polyelectrolyte assemblies," *Supramolecular Polymers, 2nd edition*, pp. 651–710, 2005.

[27] J. Borges and J. F. Mano, "Molecular interactions driving the layer-by-layer assembly of multilayers," *Chemical reviews*, vol. 114, no. 18, pp. 8883–8942, 2014.

[28] M. Schönhoff, "Layered polyelectrolyte complexes: physics of formation and molecular properties," *Journal of Physics: Condensed Matter*, vol. 15, no. 49, pp. 1781–1808, 2003.

[29] P. Lavalle, C. Gergely, F. Cuisinier, G. Decher, P. Schaaf, J. Voegel, and C. Picart, "Comparison of the structure of polyelectrolyte multilayer films exhibiting a linear and an exponential growth regime: An in situ atomic force microscopy study," *Macromolecules*, vol. 35, no. 11, pp. 4458–4465, 2002.

[30] H. G. Van de Steeg, M. A. Cohen Stuart, A. De Keizer, and B. H. Bijsterbosch, "Polyelectrolyte adsorption: a subtle balance of forces," *Langmuir*, vol. 8, no. 10, pp. 2538–2546, 1992.

[31] X. Shi, R. J. Sanedrin, and F. Zhou, "Structural characterization of multilayered dna and polylysine composite films: influence of ionic strength of dna solutions on the extent of dna incorporation," *The Journal of Physical Chemistry B*, vol. 106, no. 6, pp. 1173–1180, 2002.

[32] J. E. Wong, H. Zastrow, W. Jaeger, and R. von Klitzing, "Specific ion versus electrostatic effects on the construction of polyelectrolyte multilayers," *Langmuir*, vol. 25, no. 24, pp. 14061–14070, 2009.

[33] M. Salomäki, T. Laiho, and J. Kankare, "Counteranion-controlled properties of polyelectrolyte multilayers," *Macromolecules*, vol. 37, no. 25, pp. 9585–9590, 2004.

[34] P. Bieker and M. Schonhoff, "Linear and exponential growth regimes of multilayers of weak polyelectrolytes in dependence on ph," *Macromolecules*, vol. 43, no. 11, pp. 5052–5059, 2010.

[35] S. S. Shiratori and M. F. Rubner, "ph-dependent thickness behavior of sequentially adsorbed layers of weak polyelectrolytes," *Macromolecules*, vol. 33, no. 11, pp. 4213–4219, 2000.

[36] M. Salomäki, I. A. Vinokurov, and J. Kankare, "Effect of temperature on the buildup of polyelectrolyte multilayers," *Langmuir*, vol. 21, no. 24, pp. 11232–11240, 2005.

[37] M. Lösche, J. Schmitt, G. Decher, W. G. Bouwman, and K. Kjaer, "Detailed structure of molecularly thin polyelectrolyte multilayer films on solid substrates as revealed by neutron reflectometry," *Macromolecules*, vol. 31, no. 25, pp. 8893–8906, 1998.

[38] P. Nestler, M. Paßvogel, and C. A. Helm, "Influence of polymer molecular weight on the parabolic and linear growth regime of pdadmac/pss multilayers," *Macromolecules*, vol. 46, no. 14, pp. 5622–5629, 2013.

[39] S. Micciulla, S. Dodoo, C. Chevigny, A. Laschewsky, and R. Von Klitzing, "Short versus long chain polyelectrolyte multilayers: a direct comparison of self-assembly and structural properties," *Physical Chemistry Chemical Physics*, vol. 16, no. 40, pp. 21988–21998, 2014.

[40] Y.-H. Yang, F. A. Malek, and J. C. Grunlan, "Influence of deposition time on layer-by-layer growth of clay-based thin films," *Industrial & Engineering Chemistry Research*, vol. 49, no. 18, pp. 8501–8509, 2010.

[41] J. Schmitt, T. Gruenewald, G. Decher, P. S. Pershan, K. Kjaer, and M. Loesche, "Internal structure of layer-by-layer adsorbed polyelectrolyte films: a neutron and x-ray reflectivity study," *Macromolecules*, vol. 26, no. 25, pp. 7058–7063, 1993.

[42] G. Decher and J. B. Schlenoff, *Multilayer thin films: sequential assembly of nanocomposite materials*. John Wiley & Sons, 2006.

[43] K.-K. Chia, M. F. Rubner, and R. E. Cohen, "ph-responsive reversibly swellable nanotube arrays," *Langmuir*, vol. 25, no. 24, pp. 14044–14052, 2009.

[44] C. R. Martin, "Nanomaterials: a membrane-based synthetic approach," *Science*, vol. 266, no. 5193, pp. 1961–1966, 1994.

[45] T. Ito, Y. Matsuda, T. Jinba, N. Asai, T. Shimizu, and S. Shingubara, "Fabrication and characterization of nano porous lattice biosensor using anodic aluminum oxide substrate," *Japanese Journal of Applied Physics*, vol. 56, no. 6S1, 2017.

[46] R. Furneaux, W. Rigby, and A. Davidson, "The formation of controlled-porosity membranes from anodically oxidized aluminium," *Nature*, vol. 337, no. 6203, pp. 147–149, 1989.

[47] G. Thompson, "Porous anodic alumina: fabrication, characterization and applications," *Thin solid films*, vol. 297, no. 1-2, pp. 192–201, 1997.

[48] H. Hanot and E. Ferain, "Industrial applications of ion track technology," *Nuclear Instruments and Methods in Physics Research Section B: Beam Interactions with Materials and Atoms*, vol. 267, no. 6, pp. 1019–1022, 2009.

[49] O. Azzaroni and K. A. Lau, "Layer-by-layer assemblies in nanoporous templates: nano-organized design and applications of soft nanotechnology," *Soft Matter*, vol. 7, no. 19, pp. 8709–8724, 2011.

[50] H. Alem, F. Blondeau, K. Glinel, S. Demoustier-Champagne, and A. M. Jonas, "Layer-by-layer assembly of polyelectrolytes in nanopores," *Macromolecules*, vol. 40, no. 9, pp. 3366–3372, 2007.

[51] C. Roy, C. Dupont-Gillain, S. Demoustier-Champagne, A. M. Jonas, and J. Landoulsi, "Growth mechanism of confined polyelectrolyte multilayers in nanoporous templates," *Langmuir*, vol. 26, no. 5, pp. 3350–3355, 2009.

[52] S. Thenmozhi, N. Dharmaraj, K. Kadirvelu, and H. Y. Kim, "Electrospun nanofibers: New generation materials for advanced applications," *Materials Science and Engineering: B*, vol. 217, pp. 36–48, 2017.

[53] C. J. Roy, C. C. Buron, S. Demoustier-Champagne, and A. M. Jonas, "Nanoconfined polyelectrolyte multilayers: From nanostripes to multisegmented functional nanotubes," *Multilayer Thin Films: Sequential Assembly of Nanocomposite Materials, Second Edition*, pp. 613–636, 2012.

[54] C. Vlémincq, "Fabrication and characterization of mats made of soft lbl nanotubes," *UCL-Université Catholique de Louvain*, 2016.

[55] L. D. Peachey, "Thin sections: I. a study of section thickness and physical distortion produced during microtomy," *The Journal of Cell Biology*, vol. 4, no. 3, pp. 233–242, 1958.

[56] D. Stokes, *Principles and practice of variable pressure: environmental scanning electron microscopy (VP-ESEM)*. John Wiley & Sons, 2008.

[57] J. C. Stockert and A. Blazquez-Castro, *Fluorescence Microscopy in Life Sciences*. Bentham Science Publishers, 2017.

[58] B. R. Masters, "Handbook of biological confocal microscopy," *Journal of biomedical optics*, vol. 13, no. 2, 2008.

[59] N. A. Geisse, "Afm and combined optical techniques," *Materials Today*, vol. 12, no. 7-8, pp. 40–45, 2009.

[60] A. Rothen, "The ellipsometer, an apparatus to measure thicknesses of thin surface films," *Review of Scientific Instruments*, vol. 16, no. 2, pp. 26–30, 1945.

[61] D. A. Skoog, F. J. Holler, and S. R. Crouch, *Principles of instrumental analysis*. Cengage learning, 2017.

[62] S. Zhang, *"Layer-by-Layer Assembled Enzyme Nanotubes and Mats for Biocatalysis"*. PhD thesis, UCL-Université Catholique de Louvain, 2016.

Rue Archimède, 1 bte L6.11.01, 1348 Louvain-la-Neuve **www.uclouvain.be/epl**